Journal Pre-proofs



A comprehensive framework for multibody system analysis with clustered cables: examples of tensegrity structures

Ziyun Kan, Ningning Song, Haijun Peng, Biaosong Chen, Xueguan Song

PII: S0020-7683(20)30444-3
DOI: https://doi.org/10.1016/j.ijsolstr.2020.11.015
Reference: SAS 10912

To appear in: *International Journal of Solids and Structures*

Received Date: 23 April 2020
Revised Date: 30 September 2020
Accepted Date: 13 November 2020

Please cite this article as: Kan, Z., Song, N., Peng, H., Chen, B., Song, X., A comprehensive framework for multibody system analysis with clustered cables: examples of tensegrity structures, *International Journal of Solids and Structures* (2020), doi: https://doi.org/10.1016/j.ijsolstr.2020.11.015

This is a PDF file of an article that has undergone enhancements after acceptance, such as the addition of a cover page and metadata, and formatting for readability, but it is not yet the definitive version of record. This version will undergo additional copyediting, typesetting and review before it is published in its final form, but we are providing this version to give early visibility of the article. Please note that, during the production process, errors may be discovered which could affect the content, and all legal disclaimers that apply to the journal pertain.

© 2020 Published by Elsevier Ltd.

Journal Pre-proofs

A comprehensive framework for multibody system analysis with clustered cables: examples of tensegrity structures

Ziyun Kan[1, 2], Ningning Song[1], Haijun Peng[1*], Biaosong Chen[1], Xueguan Song[2]

1 State Key Laboratory of Structural Analysis for Industrial Equipment, Department of Engineering Mechanics, Dalian University of Technology, Dalian 116024, People's Republic of China.

2 School of Mechanical Engineering, Dalian University of Technology, Dalian 116024, People's Republic of China.

Abstract

Structures with clustered cables are widespread in many engineering applications. Most existing works involving clustered cables are based on a finite element formulation and do not address cable friction. This paper presents a novel multibody-based methodology for the mechanical analysis of systems containing clustered cable elements. The generalized coordinates of the system are chosen as configurations of the attached rigid bodies, rather than traditional nodal displacements or positions on the finite element formulation. The clustered cables are considered as internal force elements that act on the bodies. To address the friction induced by cable sliding, a comprehensive complementarity-based framework is developed for different analysis cases. For explicit dynamic analyses, by introducing a limited number of assumptions, a non-smooth LCP-based approach is proposed that enables us to integrate any mature LCP solvers into the time integration. For implicit static and dynamic analyses, a nonlinear complementarity function-based approach is proposed, which allows us to solve the problem in a unified, continuous and smooth manner. As a representative engineering application, the developed framework is employed in the mechanical analyses of active tensegrity structures. The numerical results show that the friction between the clustered cable and the struts fundamentally alters the system mechanical behavior. For static analyses, it is emphasized that friction leads to a significant difference in tension magnitudes in different segments of a clustered cable. For dynamic analyses, the results reveal that novel behavior, such as the stick-slip phenomenon of the connection points can occur frequently. The outcomes demonstrate the ability of the proposed methodology to capture the complex and diverse motion states.

Keywords: Multibody system, tensegrity structure, clustered cable, friction, Fischer-Burmeister function.

*Corresponding author. E-mail addresses: hjpeng@dlut.edu.cn .

Journal Pre-proofs

1. Introduction

In recent years, new trends in civil, mechanical, and aerospace engineering have expanded researchers' interest in novel structural designs (Nagase and Skelton, 2015; Sultan, 2009). The primary driver behind this interest is the growing demand for strong, lightweight and less expensive structures. Among these new structural styles, the tensegrity concept may be one of the most promising (Bel Hadj Ali et al., 2011; Skelton and De Oliveira, 2009). Tensegrity structures are spatial and reticulated structures composed of struts and cables. The integrity is provided by a balance between the tensional forces in cables and the compressive forces in struts (Juan and Mirats Tur, 2008). Mixing together the terms tensile and integrity emphasizes the main characteristic of this kind of structures (Cefalo and Mirats-Tur, 2011).

Given the existence of a relatively large amount of lightweight cables, tensegrity structures usually possess a high strength-to-mass ratio, which leads to a strong and lightweight structural style (Skelton and De Oliveira, 2009). This feature creates a situation where the tensegrity concept is particularly attractive for actuation and controllable structure design. Traditionally, there are two kinds of actuation strategies for tensegrity systems (Bel Hadj Ali et al., 2011; Kan et al., 2018b): the strut-based actuation (Adam and Smith, 2008; Bel Hadj Ali and Smith, 2010; Fest et al., 2004; Kanchanasaratool and Williamson, 2002) and cable-based actuation (Smaili and Motro, 2005; Wroldsen et al., 2009). Strut-based actuation directly employs telescopic struts into the structure. This actuation strategy may lead to a loss of structural stiffness before the structure is fully deployed (Bel Hadj Ali et al., 2011). Moreover, due to the size limitation of struts, it is generally difficult to meet the requirement for large shape changes using this strategy (Moored and Bart-Smith, 2009). In contrast to the strut-based strategy, the cable-based actuation strategy can maintain the structural stiffness when the structure evolves from one equilibrium configuration to another. However, this strategy possesses a high controlling complexity due to the additional control devices (Sultan and Skelton, 2003). This is of particular concern when many active cables need to be controlled in a large-scale complex structure. Moreover, a large number of embedded control devices remarkably increase the system costs, mass, and power consumption levels (Moored and Bart-Smith, 2009).

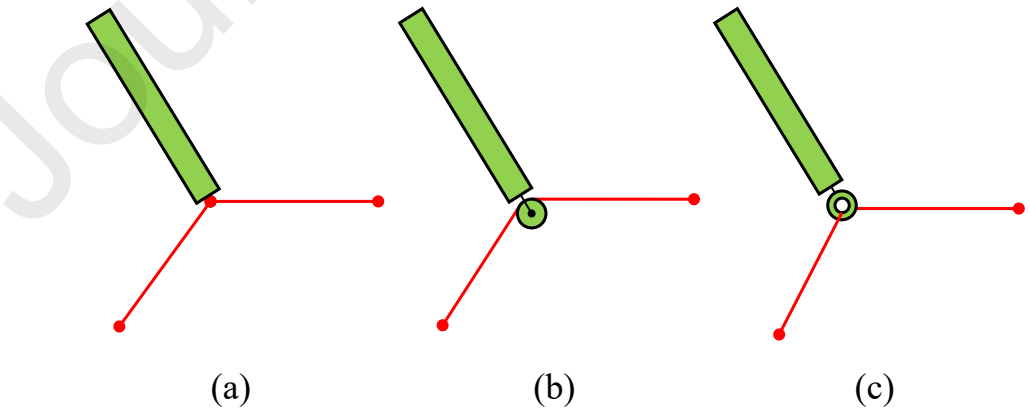


Fig. 1 A strut connected by (a) two classical cables, (b) a clustered cable passing through a pulley, (c) a clustered cable passing through a ring.

Journal Pre-proofs

The clustered cable-based actuation approach can be considered as a special kind of cable-based strategy, which inherits the advantages but to a certain extent alleviates the defects (Kan et al., 2018b). To conduct that actuation approach, the individual classical cables are clustered into continuous cables (Fig. 1). Rather than controlling multiple individual cables, clustering cables allows for the simultaneous control of cable groups using only one control device (Bel Hadj Ali et al., 2017). Moreover, the control devices can be placed outside the structure to reduce the mass of the structure. To aid the control of cable groups, sliding components such as pulleys or rings (Fig. 1 (b) and (c)) are typically installed into the system. The original concept of clustered actuation can be traced back to the 1990s when some researchers investigated the actuation of deployable pantographic structures (Kwan and Pellegrino, 1994; You and Pellegrino, 1996, 1997). Sultan and Skelton (Sultan and Skelton, 2003) first noted that the deficiency of having to control too many cables can be overcome by connecting cables together and using only one motor for control. To distinguish with classical tensegrity structures, Moored and Bart-Smith (Moored and Bart-Smith, 2009) made use of "clustered tensegrity" to denote a tensegrity activated by clustered cables. That terminology is used throughout this work.

With respect to the structural behavior of clustered tensegrity, a clustered cable passing through sliding components may lead to a redistribution of cable internal force and therefore may significantly alter the mechanical response. The key to investigating clustered tensegrity systems lies in appropriately modeling the clustered cables. Clustered/continuous/sliding cables have been applied in many other engineering applications (Bel Hadj Ali et al., 2019; Chen et al., 2010; Coulibaly et al., 2018; Gao and Lu, 2019; Ham et al., 2017; Ju and Choo, 2005; Kan et al., 2021; Lee et al., 2003; Zhang et al., 2008; Zhang et al., 2016; Zhang et al., 2015; Zhou et al., 2004). These different works all addressed the mechanics of clustered cables passing through pulleys or rings, although the scope of each was limited to the specific area that was analyzed. Different elements have been proposed regarding the number of possible sliding nodes (three-node or multi-node element), the analysis type (static and dynamic analysis), or the nonlinear finite element formulation that was used (total/updated Lagrangian, co-rotational formulation). All these works were conducted in the context of finite element methods. For the analysis of tensegrity systems using finite element methods, struts are usually considered thin and long such that they can be modeled as conventional truss elements; classical cables are modeled as special truss elements that can only sustain tensions. Over the past decades, this modeling approach has been extensively addressed by many tensegrity researchers and has been implemented in either form-finding (Aloui et al., 2019; Gan et al., 2015; Nishimura and Murakami, 2001; Pagitz and Mirats Tur, 2009; Zhang et al., 2014) or mechanical responses (Kan et al., 2018a; Kebiche et al., 1999; Murakami, 2001) analysis.

Journal Pre-proofs



(a) (b)

Fig. 2 Two typical tensegrity structures with complex-shaped struts: (a) Kenneth Snelson's **double X, (b)** tensegrity spine.

Finite element methods are indeed powerful, but may not be efficient on many occasions for the analysis of tensegrity structures. First and foremost, the struts are not necessarily thin and long. **Fig. 2** presents two typical examples: the well-known double X structure, built by Kenneth Snelson and recognized as the first reported tensegrity structure in history (Sultan, 2009), and a tensegrity spine model, a novel bionics application of this kind of structure (Myers, 2009). In both models, the cables are connected to complex-shaped struts, and there are multiple connection points between a particular strut and the cables. If one insists on using the finite element method, one must mesh the complex shaped strut with many solid elements to yield nodes at all the connection points. These nodes are shared with the cables such that existing nodal-based classical and clustered cable elements can be adopted. Such an operation would, however, greatly increase the system's degrees of freedom, leading to difficulties for rapid mechanical analysis and further structural control research. This is a reason why these classical structures have been designed for a long time but have rarely been investigated from a mechanical analysis point of view. In some cases, even if the struts are bar-like, the material and dimensional parameters of the strut, e.g., the elastic modulus and the cross-sectional area, are much greater than those of the cables. Modeling all these components by truss elements naturally leads to an whereby that the magnitude of tensile stiffness of struts is far greater than that of cables, which possibly yields an ill-conditioned stiffness matrix (Cheong et al., 2014). In addition, the rotational degree of freedom of the strut cannot be easily considered within this modeling approach.

In contrast to the finite element formulation, the multibody approach can naturally overcome the abovementioned difficulties. Considering that struts are commonly very rigid, and cables are extremely soft and light (Yang and Sultan, 2017), this approach directly models the struts as rigid bodies and models the cables as force elements connected to the bodies. These connections allow forces to be exchanged between bodies (Cefalo and Mirats-Tur, 2011). The large overall motion of a strut can be fully described by a local fixed frame, and all degrees of freedom can be inherently handled. Essentially, the dynamic behaviors of a strut are characterized by the moment of inertia in physics, regardless of the specific geometric shape. The individual classical cables and clustered cables can be linked to arbitrary material points on a particular strut rather

than only the two ends. This modeling method seems favored by tensegrity researchers with robotics or mechanical engineering backgrounds (Graells Rovira and Mirats Tur, 2009; Paul et al., 2006; Paul et al., 2005).

To address clustered cable modelling in tensegrity systems, a clustered/sliding cable element was proposed in the author's previous work (Kan et al., 2018c). The generalized coordinates of that element are chosen as the configuration for the attached bodies instead of traditional nodal displacements or positions. This type of element can be naturally integrated into multibody dynamics analysis, making it particularly suitable for analyzing systems such as clustered tensegrity structures. However, to formulate this element, it is assumed that the clustered cables can slide freely through the sliding components and that cable sliding would not lead to any tension loss. This element is able to capture the general sliding behavior between the clustered cable and the involved sliding components, and it largely simplifies the formulation in the analysis. However, the frictionless assumption is often questioned because it is merely an idealized concept that may yield unrealistic and incorrect results. This has been demonstrated both experimentally and theoretically for a wide range of engineering applications involving clustered cables. Liu et al. (Liu et al., 2014) investigated a suspen-dome structure with clustered cables, demonstrating that the deviation of tension from the value determined by the frictionless model exceeded 30% for some cables. Veuve et al. (Veuve et al., 2015; Veuve et al., 2016) studied the deployment performance of a tensegrity footbridge activated by clustered cables. Their results showed that friction has a significant influence on the motion of such kind of structure. Similar conclusions were also obtained in other engineering applications (Choo et al., 1997; Coulibaly et al., 2018; Ju and Choo, 2005). It can be concluded that considering sliding-induced friction is critical to accurately modeling the system.

The objective of this paper is to propose a general and comprehensive framework for multibody system analysis with clustered cables that considers the sliding-induced friction. This work can be considered as an extension of the author's previous work (Kan et al., 2018c). Such an extension is, however, not an easy task because considering friction fundamentally alters the mechanical behavior of the system. Friction leads to a non-uniform tension magnitude on different segments of a clustered cable. The connection points between the body and the clustered cable are of diversified motion states and may involve a stick-slip phenomenon. The sudden motion state transition inevitably introduces non-smooth properties into the system and is fully coupled with the evolution of the system configuration. This makes the problem unable to be handled continuously and smoothly, as in the frictionless case (Kan et al., 2018c), which eventually leads to the solution being hard to obtain. To address the abovementioned tricky problems induced by friction, we integrate multibody analysis with a general and comprehensive complementarity based framework. Different numerical strategies are developed for different analysis types (explicit or implicit, static or dynamic). Original theoretical developments as well as numerical and computational considerations are presented to robustly and effectively obtain the solutions. As a representative application to demonstrate versatility, the proposed framework is implemented in mechanical analyses of a clustered tensegrity system. It appears that this kind of system

is seldom addressed from a mechanical analysis point of view, but can be easily assessed by using the proposed framework.

2. Brief review of the complementarity theory

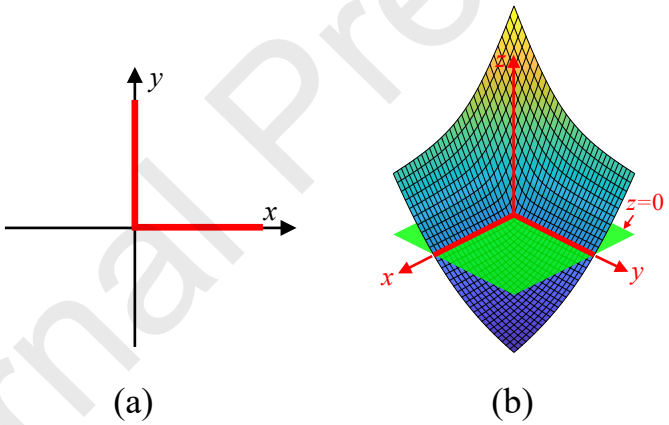
In this section, we present some brief reviews of the complementarity theory relevant to the present work. For more details, interested readers are referred to (Pang and Facchinei, 2003).

2.1 Complementarity relationship and complementarity function

Definition. Two real numbers x and y are said to have a complementarity relationship if and only if the following relationship holds

$$x \geq 0, y \geq 0, xy = 0 \tag{1}$$

In other words, x and y have a complementarity relationship if and only if point (x, y) is located on the two nonnegative semiaxes of the oxy coordinate system, as shown in Fig. 3 (a). It is clear that the relationship between x and y cannot be given as an explicit formulation such as $y = f(x)$. However, one can reformulate the complementarity relationship by using an implicit function.



(a) (b)

Fig. 3 (a) Complementarity relationship, (b) Fischer-Burmeister function.

Definition. A continuous function with two variables, $\psi : \Re^2 \to \Re^1$, is a complementarity function if for any pair $(x, y) \in \Re^2$

$$\psi(x, y) = 0 \Leftrightarrow [x \geq 0, y \geq 0, xy = 0] \tag{2}$$

where the symbol "$\Leftrightarrow$" means "equivalent to". There are many complementarity functions available, and the most well-known is the following

$$\psi_{\mathrm{FB}}(x, y) = \sqrt{x^2 + y^2} - (x + y) \tag{3}$$

where "FB" denotes "Fischer-Burmeister" originally proposed in (Fischer, 1992). Fig. 3 (b) shows a graph of the complementarity function, which clearly demonstrates the

Journal Pre-proofs

complementarity relationship for any pair of solutions $\psi(x,y)=0$. It is noteworthy that the function ψ_{FB} is convex and smooth/differentiable almost everywhere except at point $(0,0)$.

2.2 The step-like function

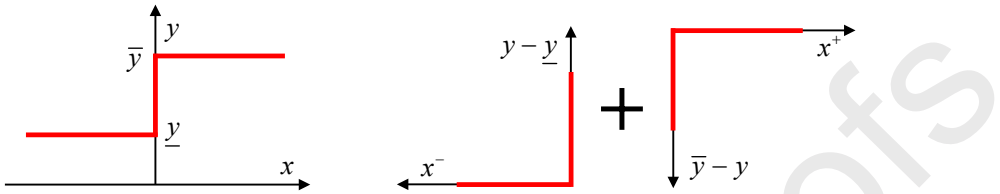


Fig. 4 (a) The step-like function, and (b) its reformulation.

The step-like function is widely used in representing a frictional contact problem, such as in the classical Coulomb's law of friction (Jean, 1999). As shown in Fig. 4 (a), it is defined piecewise as

$$y\begin{cases}=\bar{y} & \text{if } x>0\\ \in\left[\underline{y},\bar{y}\right] & \text{if } x=0\\ =\underline{y} & \text{if } x<0\end{cases} \tag{4}$$

where $\bar{y}$ and $\underline{y}$ are the upper and lower bounds, respectively, and x is the conditional value. To reformulate the step-like function, two assistant variables x^+ and x^- can be introduced, and the step-like function can be expressed by two pairs of standard complementarity relationships

$$\begin{cases}x^+\ge 0,\bar{y}-y\ge 0,x^+\left(\bar{y}-y\right)=0\\ x^-\ge 0,y-\underline{y}\ge 0,x^-\left(y-\underline{y}\right)=0\end{cases} \tag{5}$$

with an additional relationship

$$x=x^+-x^- \tag{6}$$

Interested readers are referred to (Zheng and Li, 2015) for a detailed explanation of the equivalence between Eq. (4) and Eqs. (5) and (6). As indicated in Fig. 4 (b), the assistant variables x^+ and x^- actually correspond to the conditional value x that maps to the positive direction ($\left(|x|+x\right)/2$) and to the negative direction ($\left(|x|-x\right)/2$), respectively. The graph shown in Fig. 4 (a) can be visualized as an intersection of the three hypersurfaces defined by Eqs. (5) and (6) in the four-dimensional space $\Re^4$: $\left\{x,y,x^+,x^-\right\}$. Once x^+ and x^- are solved, by substituting them into Eq. (6), we can establish the relationship between x and y.

Journal Pre-proofs

2.3 Linear complementarity problem

Definition. A linear complementarity problem (LCP) seeks the solutions of $\boldsymbol{z} \in \Re^n$ subjected to the following equality and inequality conditions:

$$\begin{cases} \boldsymbol{w} = \boldsymbol{A}\boldsymbol{z} + \boldsymbol{b} \\ \boldsymbol{w} \geq \boldsymbol{0}, \boldsymbol{z} \geq \boldsymbol{0}, \boldsymbol{w}^{\mathrm{T}}\boldsymbol{z} = 0 \end{cases} \tag{7}$$

where $\boldsymbol{b} \in \Re^n$ is an n-dimensional column vector, $\boldsymbol{A} \in \Re^{n \times n}$ is a given square matrix of dimension n, and the vector $\boldsymbol{v} \geq \boldsymbol{0}$ ($\boldsymbol{v} = \boldsymbol{w}, \boldsymbol{z}$) means that each component of $\boldsymbol{v}$ is nonnegative. The above LCP is denoted by the pair LCP($\boldsymbol{A}$, $\boldsymbol{b}$).

The inequality complementary condition in expression (7) is commonly written in a compact form:

$$\boldsymbol{0} \leq \boldsymbol{w} \perp \boldsymbol{z} \geq \boldsymbol{0} \tag{8}$$

where $\boldsymbol{w} \perp \boldsymbol{z}$ denotes $\boldsymbol{w}^{\mathrm{T}}\boldsymbol{z} = 0$. According to the nonnegative characteristic of $\boldsymbol{z}$ and $\boldsymbol{w}$, the complementary relationship $w_i z_i = 0$ holds for every single component. An LCP can have a unique solution, multiple solutions or no solution at all. From the above complementary relationship, it follows that when $w_i > 0$, then $z_i = 0$, and vice versa. This implies that one can use an exhaustive method to find out all existing solutions, which treats the problem by a combinatorial evolution of the complementary relationship $w_i z_i = 0$. An LCP of dimension n provides 2^n different combination cases. For a problem of large dimensions, the exhaustive method becomes numerically expensive as 2^n grows rapidly. A more efficient approach uses the complementary pivot algorithm, commonly referred to as the Lemke's algorithm (Lemke, 1965). Other efficient algorithms for solving an LCP can be found in (Cottle et al., 1992). If special LCP solvers are not available, one can use a nonlinear optimization solver to find the solution, which can be done by first transforming the original LCP($\boldsymbol{A}$,$\boldsymbol{b}$) into the quadratic programming problem:

$$\begin{cases} \text{minimize} & \boldsymbol{z}^{\mathrm{T}}\left(\boldsymbol{A}\boldsymbol{z} + \boldsymbol{b}\right) \\ \text{subject to} & \boldsymbol{A}\boldsymbol{z} + \boldsymbol{b} \geq \boldsymbol{0}, \boldsymbol{z} \geq \boldsymbol{0} \end{cases} \tag{9}$$

If LCP($\boldsymbol{A}$, $\boldsymbol{b}$) has a solution, such a solution must be the solution of the quadratic programming (9) as well, and it corresponds to a target value zero.

3. Explicit dynamic analysis of a multibody system with clustered cable elements

In this section, explicit dynamic analysis of multibody system with clustered cables is presented in the context of an analysis of tensegrity systems.

3.1 Basic kinematic descriptions and general equations

First, we declare that we make use of the following modeling assumptions throughout this paper.

(1) The struts in the system can of arbitrary shape, i.e., they are not limited to bar-like shapes, but should be sufficiently thick such that the overall deformations can be neglected.

Journal Pre-proofs

(2) The classical and clustered cables are perfectly flexible, slender and light such that bending effects and inertial effects can be neglected. Every segment of a clustered cable remains straight in tension.
(3) The sliding components for the clustered cables, such as pulleys or rings, are sufficiently small. As a result, the connection points between the cables and the struts can be considered fixed to the struts.
(4) A strut cannot slide across an adjacent strut along the clustered cable, which means that the order of the connection points along the clustered cable remains unchanged.
(5) Deformations of the clustered cables are considered small. Cable damping is not considered. A linear elastic constitutive relation is used.

Based on the above assumptions, a strut in the system can be considered as a rigid body. The classical and the clustered cables are considered as force elements that interact with rigid bodies. Fig. 5 shows a single rigid body with an index i located in three-dimensional Cartesian space. $OXYZ$ denotes the global coordinate frame, and $o_i x_i y_i z_i$ denotes the local coordinate frame fixed to the body. The generalized coordinates of the body can be defined by the configuration of the local coordinate frame

$$\boldsymbol{q}_i = \begin{bmatrix} \boldsymbol{R}_i^{\mathrm{T}} & \boldsymbol{\Theta}_i^{\mathrm{T}} \end{bmatrix}^{\mathrm{T}} \tag{10}$$

where $\boldsymbol{R}_i \in \Re^3$ denotes the position vector for the origin of the local coordinate frame. $\boldsymbol{\Theta}_i$ represents the orientation coordinates of the local coordinate frame, which can be expressed by the Euler or Cardan angle (Shabana, 2005). Throughout this work, we adopt the classical Euler angle as the orientation coordinates. Six generalized coordinates ($\boldsymbol{q}_i \in \Re^6$) are needed to describe the configuration of a single body. The generalized velocities of the body can be obtained by taking the derivative of the generalized coordinates with respect to time,

$$\dot{\boldsymbol{q}}_i = \begin{bmatrix} \dot{\boldsymbol{R}}_i^{\mathrm{T}} & \dot{\boldsymbol{\Theta}}_i^{\mathrm{T}} \end{bmatrix}^{\mathrm{T}} \tag{11}$$

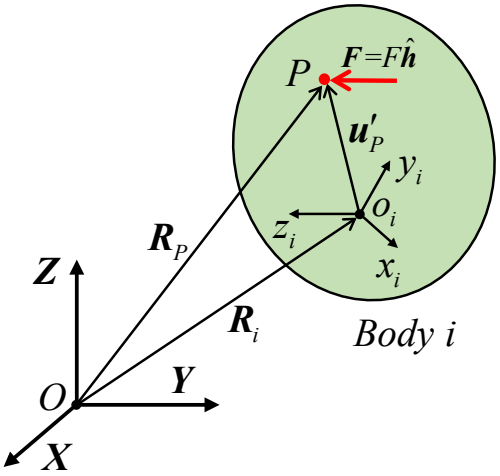


Fig. 5 A rigid body in three-dimensional Cartesian space.

Journal Pre-proofs

As shown in Fig. 5, an arbitrary material point *P* located at the body can be uniquely identified by a vector $\boldsymbol{u}'_P \in \Re^3$, that is the position vector of $\overrightarrow{o_i P}$ whose components are measured in the *local* coordinate frame. Throughout this paper, the notation $(\bullet)'$ denotes a quantity that is measured in the related *local* coordinate frame. It is obvious that $\boldsymbol{u}'_P$ is a constant regardless of whether the rigid body is being fixed in the space or is undergoing a large overall motion.

The position vector of point *P* measured in the *global* coordinate frame ($\overrightarrow{OP}$) can be calculated as:

$$\boldsymbol{R}_P = \boldsymbol{R}_i + \boldsymbol{A}_i \boldsymbol{u}'_P \tag{12}$$

where $\boldsymbol{A}_i \in \Re^{3\times 3}$, a function of the orientation coordinates $\boldsymbol{\Theta}_i$, is the orthogonal transformation matrix between the local coordinate frame and the global coordinate frame. Taking the derivative of Eq. (12) with respect to the time yields the absolute velocity vector of the material point *P*.

$$\boldsymbol{v}_P = \dot{\boldsymbol{R}}_P = \boldsymbol{B}_P \dot{\boldsymbol{q}}_i \tag{13}$$

where matrix $\boldsymbol{B}_P \in \Re^{3\times 6}$ can be computed as (Shabana, 2005)

$$\boldsymbol{B}_P = \partial \boldsymbol{R}_P / \partial \boldsymbol{q}_i = \begin{bmatrix} \boldsymbol{I}_3 & -\boldsymbol{A}_i \tilde{\boldsymbol{u}}'_P \boldsymbol{G}'_i \end{bmatrix} \tag{14}$$

where $\boldsymbol{I}_3 \in \Re^{3\times 3}$ is the third-order identity matrix, $\tilde{\boldsymbol{u}}'_P \in \Re^{3\times 3}$ is an antisymmetric matrix relevant to the vector $\boldsymbol{u}'_P$, and $\boldsymbol{G}'_i \in \Re^{3\times 3}$ is a transition matrix between the angular velocity and generalized velocity.

For a multibody system composed of *m* bodies, the generalized coordinates can be directly chosen as an aggregate of the generalized coordinates of each single body, as

$$\boldsymbol{q} = \begin{bmatrix} \boldsymbol{q}_1^{\mathrm{T}} & \boldsymbol{q}_2^{\mathrm{T}} & \cdots & \boldsymbol{q}_m^{\mathrm{T}} \end{bmatrix}^{\mathrm{T}} \tag{15}$$

Based on the theory of the Lagrangian equation of motion, the system governing equation can be derived as the following index-3 differential-algebraic equations (DAEs) (Shabana, 2005):

$$\begin{cases} \boldsymbol{M}(\boldsymbol{q})\ddot{\boldsymbol{q}} + \boldsymbol{\Phi}_{\boldsymbol{q}}^{\mathrm{T}} \boldsymbol{\lambda} + \boldsymbol{Q}_{\mathrm{i}}(\boldsymbol{q}, \dot{\boldsymbol{q}}) - \boldsymbol{Q}_{\mathrm{e}}(\boldsymbol{q}, \dot{\boldsymbol{q}}) = \boldsymbol{0} \\ \boldsymbol{\Phi}(\boldsymbol{q}, t) = \boldsymbol{0} \end{cases} \tag{16}$$

where $\boldsymbol{M}$ is the mass matrix, $\boldsymbol{\Phi}$ is the constraint equation, $\boldsymbol{\Phi}_{\boldsymbol{q}}$ is the Jacobian matrix of the constraint equation, $\boldsymbol{\lambda}$ is the Lagrange multiplier vector physically representing the constraint force, $\boldsymbol{Q}_{\mathrm{i}}$ is the quadratic velocity vector (the sum of Coriolis and

centrifugal forces) and $\boldsymbol{Q}_{\mathrm{e}}$ is the generalized "external" force vector that is induced by various kinds of force, such as the external concentrated forces, the forces in classical cables and, the main concern in this work, the clustered cables.

By using the principle of virtual work, we can obtain the generalized force vector of a concentrated force, which is important for the following deduction of the cable element. As shown in Fig. 5, a concentrated force is applied on the rigid body. The action point of the force is fixed to material point *P*, and the magnitude and the direction are denoted as $F \in \Re$ and $\hat{\boldsymbol{d}} \in \Re^3$, respectively (throughout this paper, the notation $\hat{(\bullet)}$ denotes a unit direction vector). The virtual work done by the concentrated force yields

$$\delta W = \boldsymbol{F}^{\mathrm{T}} \delta \boldsymbol{R}_P \tag{17}$$

where $\boldsymbol{F} = F\hat{\boldsymbol{h}}$ is the global force vector, and $\delta \boldsymbol{R}_P$ is the global virtual displacement of the force action point under a variation of the generalized coordinates ($\delta \boldsymbol{q}_i$). By using Eq. (14), we can establish the relationship $\delta \boldsymbol{R}_P = \boldsymbol{B}_P \delta \boldsymbol{q}_i$, and the generalized force vector of the concentrated force yields

$$\boldsymbol{Q}_c = F\boldsymbol{B}_P^{\mathrm{T}}\hat{\boldsymbol{h}} \tag{18}$$

The detailed expressions of the mass matrix, the quadratic velocity vector and the generalized force vector contributed by other kinds of forces (e.g., torques) can be found in (Shabana, 2005)

For a typical tensegrity system, the constraint equation $\boldsymbol{\Phi}$ may consist of three parts. The first part is induced by the non-independent orientation coordinates. This part vanishes for the current Euler angle based orientation coordinates. The second part is induced by the ball joints for a class *k* ($k \geq 2$) (Skelton and De Oliveira, 2009) tensegrity system. The third part is induced by the actuation of some components, as well as the boundary constraints. For detailed expressions of these constraint equations and the related constraint Jacobian matrices, the readers are referred to the author's previous work (Kan et al., 2018c).

Eq. (16) represents the dynamic equation of the entire system. When no constraint exists, the dynamics equation (16) degenerates into to a set of ordinary differential equations (ODEs). For static analyses, by dropping the items of the generalized velocities ($\dot{\boldsymbol{q}}$) and accelerations ($\ddot{\boldsymbol{q}}$), we can obtain the static equilibrium equation of the system which is a set of nonlinear algebraic equations.

$$\begin{cases} \boldsymbol{\Phi}_{\boldsymbol{q}}^{\mathrm{T}}\boldsymbol{\lambda} - \boldsymbol{Q}_{\mathrm{e}}(\boldsymbol{q}) = \boldsymbol{0} \\ \boldsymbol{\Phi}(\boldsymbol{q}) = \boldsymbol{0} \end{cases} \tag{19}$$

Journal Pre-proofs

At this point, general static and dynamic equations are formulated. The core task in the following section is to establish the relationship between the generalized coordinates ($\boldsymbol{q}$) and the generalized force vector ($\boldsymbol{Q}$) for a clustered cable element. Robust and effective treatments in numerically solving the dynamic equation (16) and the static equilibrium equation (19) are emphatically discussed when considering the sliding-induced friction in the clustered cable element.

3.2 Explicit dynamic analysis with clustered cable elements

The dynamic equation (16) can be solved using either explicit algorithms or implicit algorithms. For explicit algorithms, a commonly used approach is first transforming the dynamic equation (16) into an index-1 DAEs (Hairer and Wanner, 2002) by taking the derivative of the constraint equations twice, and then applying any explicit time integration schemes, such as the explicit Runge-Kutta or explicit Euler schemes, to solve the equation. To enforce a satisfaction of the constraint equation at the position level, constraint stabilization approaches, such as the popular Baumgarte's technique (Baumgarte, 1972) can be found. In the analysis of each time step, the core task related to the clustered cable element is to calculate the generalized force vector based on a newly-updated configuration. In the following section, we focus on this core task.

3.2.1 General formulation of the generalized force vector

As shown in Fig. 6, let us consider a clustered cable connected with m rigid bodies. The cable consists of n segments. The number of sliding components in the cable is n-1, and the number of connection points between the entire element and the rigid bodies is n+1. It is worth mentioning that m is not necessarily equal to n+1 since some of the connection points may be located on the same rigid body (but at different material points). The connection points between the clustered cable and the rigid bodies are denoted as P_1, P_2, …, P_{n+1}, respectively. Connection points P_2, …, P_n are the possible sliding connection points. The position vectors of the connection points measured in the respective local coordinate frame are denoted as $\boldsymbol{u}_1', \boldsymbol{u}_2', \ldots, \boldsymbol{u}_{n+1}'$, respectively. These local position vectors are constants throughout the analysis, according to the previous assumptions (the sliding components are sufficiently small).

Journal Pre-proofs

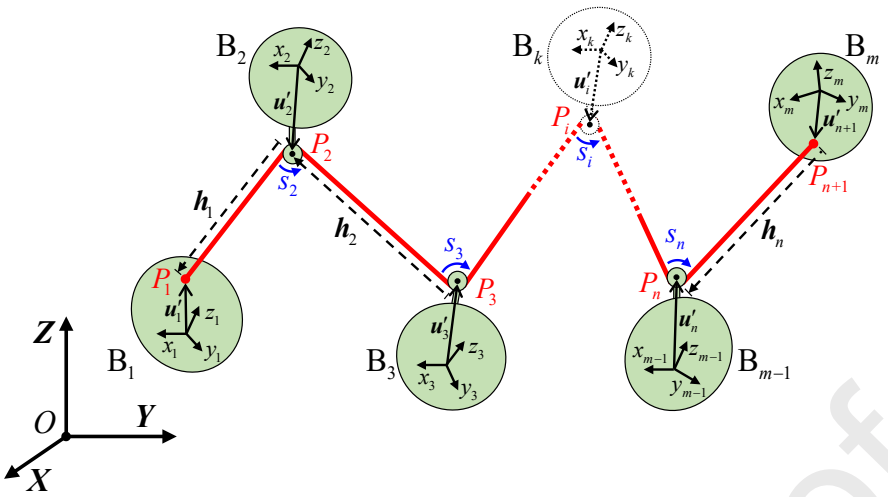


Fig. 6 A multibody system containing a clustered cable element.

At the analysis of the current *k*th time step, the newly updated configuration (the generalized coordinates) of the system is assumed as

$$\boldsymbol{q}^{(k)} = \left[\boldsymbol{q}_1^{(k)\mathrm{T}} \quad \boldsymbol{q}_2^{(k)\mathrm{T}} \quad \cdots \quad \boldsymbol{q}_m^{(k)\mathrm{T}} \right]^{\mathrm{T}} \tag{20}$$

By using Eq. (12), we can first obtain the global position vectors of the connection points, $\boldsymbol{R}_{P_i} \in \Re^3 \left(1 \le i \le n+1\right)$. For the *i*th $\left(1 \le i \le n\right)$ segment of the clustered cable element, define $\boldsymbol{h}_i \in \Re^3$ as the segment vector $\overrightarrow{P_{i+1}P_i}$, and define $\hat{\boldsymbol{h}}_i \in \Re^3$ and $h_i \in \Re$ as the unit vector and the length of the vector $\overrightarrow{P_{i+1}P_i}$. All these items are measured in the global coordinate frame. It is easy to compute that

$$\boldsymbol{h}_i = \boldsymbol{R}_{P_i} - \boldsymbol{R}_{P_{i+1}} \tag{21}$$

$$h_i = \sqrt{\boldsymbol{h}_i^{\mathrm{T}} \boldsymbol{h}_i} \tag{22}$$

$$\hat{\boldsymbol{h}}_i = \boldsymbol{h}_i / h_i \tag{23}$$

Clearly, the unit vector $\hat{\boldsymbol{h}}_i$ and its opposite $-\hat{\boldsymbol{h}}_i$ denote the direction of the tension forces of the *i*th $\left(1 \le i \le n\right)$ segment that act on the two bodies with which the segment connects. h_i represents the deformed length of the segment. To establish the relationship between the generalized coordinates ($\boldsymbol{q}$) and the generalized force vector of the clustered cable element, the remaining core task is to compute the tension magnitude of each segment. If the clustered cable is assumed to run over frictionless pulleys or rings, the tension magnitude of each segment is exactly the same. The axial deformation of the entire clustered cable element can be obtained by directly summing the deformed length of each segment and then subtracting the free/undeformed length of the entire clustered cable element. The tension magnitude of the cable element as

Journal Pre-proofs

well as that of each segment can be calculated straightforwardly by using the constitutive law, as did in many existing works (Bel Hadj Ali et al., 2011; Boulaud et al., 2020; Chen et al., 2010; Kan et al., 2018c). There is no need to explore trivial details such as whether a particular connection point is sliding or sticking, or which direction does it slide towards if a sliding motion indeed occurs. This approach, however, does not apply for the frictional case. Due to friction, tension magnitude differences are allowed, and one must carefully track the motions of each possible sliding connection point, as given below.

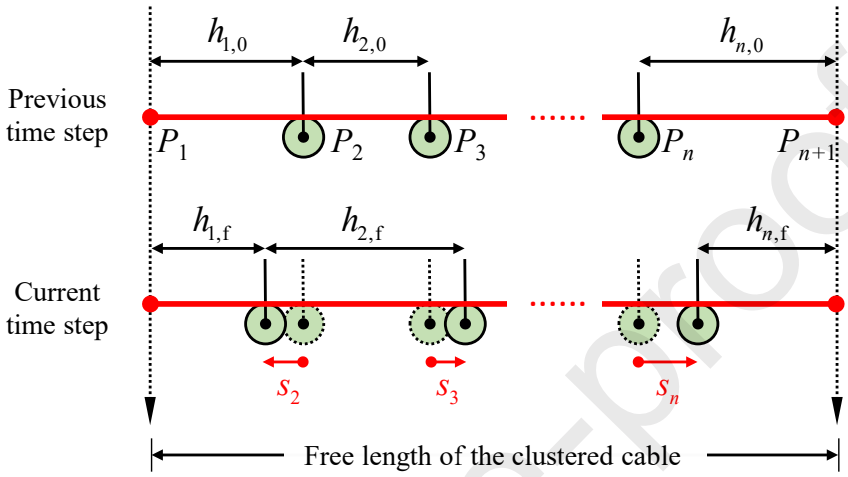


Fig. 7 Sliding motion of connection points occurring in a time step.

Note that for the analysis of the current *k*th time step, every information is known at the previous *k*-1th time step. This information includes: the system configuration ($\boldsymbol{q}^{(k-1)}$) and the free length of each segment (for the *i*th segment denoted as $h_{i,0}$), which can be obtained by tracking the time history of the sliding magnitude of each connection point.

To obtain the tension magnitude of each segment, we can first introduce an *unknown* instantaneous sliding magnitude vector $\boldsymbol{s} \in \Re^{n-1}$

$$\boldsymbol{s} = \begin{bmatrix} s_2 & s_3 & \cdots & s_n \end{bmatrix}^{\mathrm{T}} \tag{24}$$

where s_i $(2 \le i \le n)$ represents the sliding magnitude of the *i*th connection point (P_i) towards the end connection point (P_{n+1}) that occurs from the last time step to the current time step. These sliding magnitudes are all measured with respect to the free length of the clustered cable. Clearly, a negative value of s_i represents that the connection point has slid towards the first connection point (P_1), and $s_i = 0$ denotes that no sliding motion occurs and the cable is sticking.

The free length ($h_{i,\mathrm{f}}$) of the *i*th segment for the current *k*th time step can be updated by taking into account the sliding motions of the related connection points.

Journal Pre-proofs

$$h_{i,\mathrm{f}} = \begin{cases} h_{1,0} + s_2 & i = 1 \\ h_{i,0} - s_i + s_{i+1} & 2 \le i \le n-1 \\ h_{n,0} - s_n & i = n \end{cases} \tag{25}$$

The tension magnitude of each segment can be obtained by using the constitutive law, as

$$F_i = EA\varepsilon_i \tag{26}$$

where EA is the tensile stiffness, and ε_i is the axial strain. The engineering strain is commonly used for clustered cable analysis for the frictionless case, which yields

$$\varepsilon_i = \frac{h_i - h_{i,\mathrm{f}}}{h_{i,\mathrm{f}}} \tag{27}$$

However, if we directly adopt the above engineering strain in the frictional case, we can find that the tension magnitude has a *nonlinear* relationship with sliding magnitude which will largely complicate the current explicit dynamic analysis, as will be shown below. To simplify the formulation, we introduce an important approximation in the strain calculation for the current explicit dynamic analysis.

$$\varepsilon_i \approx \frac{h_i - h_{i,\mathrm{f}}}{h_i} \tag{28}$$

It can be proved that for small deformation analyses ($\Delta h = h_i - h_{i,\mathrm{f}} \ll h_i\left(h_{i,\mathrm{f}}\right)$), errors caused by the approximation are negligible. Once the tension magnitude of each segment of the clustered cable is obtained, the generalized force vector can be formulated via the following procedure.

For each connection point P_i, compute the corresponding matrix $\boldsymbol{B}_{P_i} = \partial \boldsymbol{R}_{P_i} / \partial \boldsymbol{q}_{\mathrm{b}(i)} \in \Re^{3\times 6}$ using Eq. (14), where $\boldsymbol{q}_{\mathrm{b}(i)}$ denotes the configuration (generalized coordinates) of the rigid body at which the connection point is located. For every segment of the clustered cable, define a corresponding constant mapping matrix $\boldsymbol{C}_i \in \Re^{2\times m}$. Taking the ith segment as an example, the corresponding segment vector is $\boldsymbol{h}_i = \overrightarrow{P_{i+1}P_i}$. If the connection points P_i and P_{i+1} are located at body p and body q, respectively, we have $\boldsymbol{C}_i(1,p) = \boldsymbol{C}_i(2,q) = 1$, and all the other items in matrix $\boldsymbol{C}_i$ are zeroes. It can be verified that

$$\begin{cases} \boldsymbol{q}_p = \left(\boldsymbol{C}_i(1,:) \otimes \boldsymbol{I}_6\right)\boldsymbol{q} \\ \boldsymbol{q}_q = \left(\boldsymbol{C}_i(2,:) \otimes \boldsymbol{I}_6\right)\boldsymbol{q} \end{cases} \tag{29}$$

where $\otimes$ is the Kronecker product and $\boldsymbol{I}_6$ is the 6×6 identity matrix.

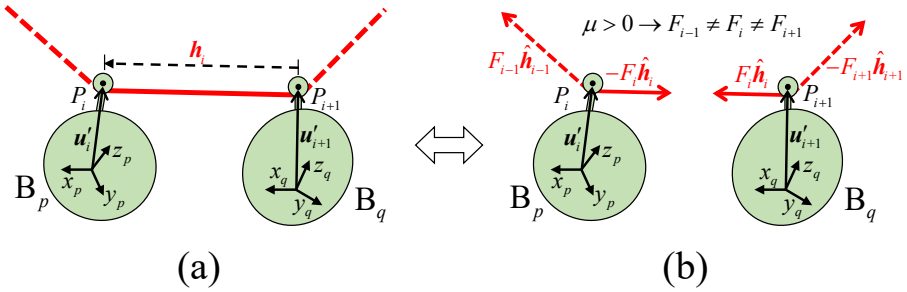


Fig. 8 (a) A segment of the clustered cable, and (b) the equivalent concentrated forces.

As illustrated in Fig. 8, the tension force in a segment can be equivalent to a pair of concentrated forces. By taking advantage of Eq. (18), we can first obtain the generalized force vector of each segment.

$$\boldsymbol{Q}_{\mathrm{e}}^{(i)}\left(\boldsymbol{q}_p,\boldsymbol{q}_q,s_i,s_{i+1}\right)=\begin{bmatrix}\boldsymbol{Q}_p^{(i)}\\ \boldsymbol{Q}_q^{(i)}\end{bmatrix}=\begin{bmatrix}-F_i\boldsymbol{B}_i^{\mathrm{T}}\hat{\boldsymbol{h}}_i\\ F_i\boldsymbol{B}_{i+1}^{\mathrm{T}}\hat{\boldsymbol{h}}_i\end{bmatrix} \tag{30}$$

where $\hat{\boldsymbol{h}}_i$ is the unit vector of $\overrightarrow{P_{i+1}P_i}$ and $\boldsymbol{B}_i$ and $\boldsymbol{B}_{i+1}$ are the matrices associated with connection points P_i and P_{i+1}, respectively. Assembling the generalized force vector of each segment into a system level by using the mapping matrix $\boldsymbol{C}_i$, we have

$$\boldsymbol{Q}_{\mathrm{e}}\left(\boldsymbol{q},\boldsymbol{s}\right)=\sum_{i=1}^{n}\left(\boldsymbol{C}_i\otimes\boldsymbol{I}_6\right)^{\mathrm{T}}\boldsymbol{Q}_{\mathrm{e}}^{(i)} \tag{31}$$

The above expression represents a general formulation of the generalized force vector contributed by the clustered cable element. It is of particular importance to note that the expression is not only a function of the system configuration $\boldsymbol{q}\left(=\boldsymbol{q}^{(k)}\right)$ but also a function of the sliding magnitude vector $\boldsymbol{s}$. To complete the calculation, the next step is to obtain the unknown sliding magnitude variable $\boldsymbol{s}$, as given below.

3.2.2 Determination of the sliding magnitude vector

To calculate the sliding magnitude vector, a sliding criterion must be introduced, which defines a sliding limit for the tension magnitudes of two sides of a particular connection point. The most widely used sliding criterion is the Euler-Eytelwein equation, also known as the capstan equation, which states the following relationship.

$$T_2=\mathrm{e}^{-\mu\theta}T_1 \tag{32}$$

where T_1 and T_2 are the tension magnitudes of two sides of a particular connection point; $\mathrm{e}^{-\mu\theta}$ denotes the tension ratio at the sliding limit state and θ (as indicated in Fig. 9) and μ are the total contact angle and the friction coefficient between the

contact component and the cable, respectively. This sliding criterion can be derived from the classical Coulomb's law of friction. Detailed derivations can be found in (Beer and Johnston, 1996).

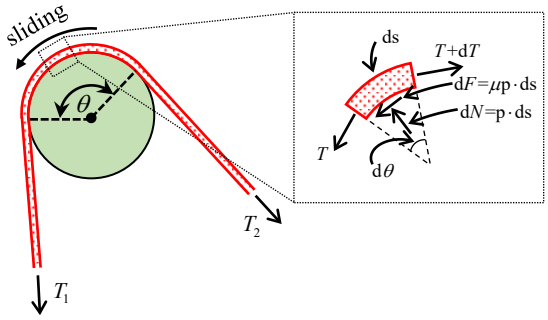


Fig. 9 A clustered cable passing through a circular sliding component.

It is important to note that the equal sign in Eq. (32) implies a limit state that the cable is sliding or on the verge of sliding. Depending on the ratio of the tension magnitudes, sliding might or might not occur. By implementing this criterion and considering that the cable may slide to either side for a particular connection point, or even not slide at all, we have three situations for every possible sliding connection point.

$$F_{i-1}/F_i \begin{cases} = 1/\alpha_i & \text{if } s_i > 0 \\ \in [\alpha_i, 1/\alpha_i] & \text{if } s_i = 0 \\ = \alpha_i & \text{if } s_i < 0 \end{cases} \tag{33}$$

where $\alpha_i = \mathrm{e}^{-\mu_i \theta_i}$ $(2 \le i \le n)$, which can be calculated from the current updated system configuration $\boldsymbol{q}^{(k)}$. The introduction of the sliding criterion yields a set of inequality or equality constraints for the motion states of the connection points. For a clustered cable element with multiple connection points, tension magnitudes in different segments are fully coupled through the sliding criterion, and one cannot determine the unknown sliding magnitude t independently or recursively for each single connection point from Eq. (33). To obtain the solutions robustly and effectively, we use a linear complementarity approach, as given below.

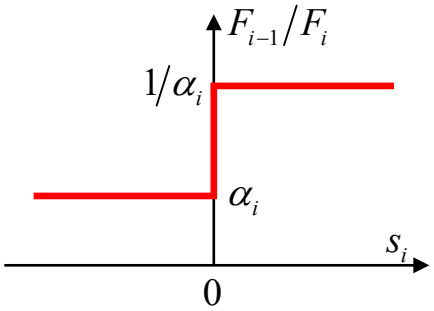


Fig. 10 Formulate the relationship between the tension magnitude ratio and the sliding magnitude using a step-like function.

As illustrated in Fig. 10, system (33) is a step-like function. According to Section

2.2, by introducing two assistant variables s_i^+ and s_i^-, system (33) can be transformed into two pairs of standard complementarity relationships

$$\begin{cases} s_i^+ \geq 0, \overline{\varsigma}_i^+ \geq 0, s_i^+ \overline{\varsigma}_i^+ = 0 \\ s_i^- \geq 0, \overline{\varsigma}_i^- \geq 0, s_i^- \overline{\varsigma}_i^- = 0 \end{cases} \tag{34}$$

with an additional relationship

$$s_i = s_i^+ - s_i^- \tag{35}$$

where

$$\begin{cases} \overline{\varsigma}_i^+ = 1/\alpha_i - F_{i-1}/F_i \\ \overline{\varsigma}_i^- = F_{i-1}/F_i - \alpha_i \end{cases} \tag{36}$$

Note that the cable cannot get slack ($F_i > 0$), to simplify the formulation, complementarity variables $\overline{\varsigma}_i^+$ and $\overline{\varsigma}_i^-$ can be scaled up by multiplying F_i.

$$\begin{cases} \varsigma_i^+ = F_i/\alpha_i - F_{i-1} \\ \varsigma_i^- = F_{i-1} - \alpha_i F_i \end{cases} \tag{37}$$

To write the complementary relationships on an elemental level, we can define the following assistant vectors by collecting the intermediate variables:

$$\boldsymbol{s}^+ = \left[s_2^+, s_3^+, ..., s_n^+ \right]^{\mathrm{T}} \in \Re^{(n-1)} \tag{38}$$

$$\boldsymbol{s}^- = \left[s_2^-, s_3^-, ..., s_n^- \right]^{\mathrm{T}} \in \Re^{(n-1)} \tag{39}$$

$$\boldsymbol{\varsigma}^+ = \left[\varsigma_2^+, \varsigma_3^+, ..., \varsigma_n^+ \right]^{\mathrm{T}} \in \Re^{(n-1)} \tag{40}$$

$$\boldsymbol{\varsigma}^- = \left[\varsigma_2^-, \varsigma_3^-, ..., \varsigma_n^- \right]^{\mathrm{T}} \in \Re^{(n-1)} \tag{41}$$

As a result, we have

$$\boldsymbol{s} = \boldsymbol{s}^+ - \boldsymbol{s}^- \tag{42}$$

, and the complementarity relationship (34) can be transformed into

$$\begin{cases} 0 \leq \boldsymbol{s}^+ \perp \boldsymbol{\varsigma}^+ \geq 0 \\ 0 \leq \boldsymbol{s}^- \perp \boldsymbol{\varsigma}^- \geq 0 \end{cases} \tag{43}$$

Substituting expressions (25), (26) and (28) into expression (37), and writing it in a matrix form yields

$$\begin{cases} \boldsymbol{\varsigma}^+ = \boldsymbol{A}^+ \boldsymbol{s} + \boldsymbol{b}^+ \\ \boldsymbol{\varsigma}^- = -\boldsymbol{A}^- \boldsymbol{s} + \boldsymbol{b}^- \end{cases} \tag{44}$$

where

Journal Pre-proofs

$$\boldsymbol{A}^{+}=\begin{bmatrix} k_1+k_2/\alpha_2 & -k_2/\alpha_2 & & & \\ -k_2 & k_2+k_3/\alpha_3 & -k_3/\alpha_3 & & \\ & \cdots & \cdots & \cdots & \\ & & -k_{n-2} & k_{n-2}+k_{n-1}/\alpha_{n-1} & -k_{n-1}/\alpha_{n-1} \\ & & & -k_{n-1} & k_{n-1}+k_n/\alpha_n \end{bmatrix} \tag{45}$$

$$\boldsymbol{A}^{-}=\begin{bmatrix} k_1+\alpha_2 k_2 & -\alpha_2 k_2 & & & \\ -k_2 & k_2+\alpha_3 k_3 & -\alpha_3 k_3 & & \\ & \cdots & \cdots & \cdots & \\ & & -k_{n-2} & k_{n-2}+\alpha_{n-1}k_{n-1} & -\alpha_{n-1}k_{n-1} \\ & & & -k_{n-1} & k_{n-1}+\alpha_n k_n \end{bmatrix} \tag{46}$$

and

$$\boldsymbol{b}^{+}=\begin{bmatrix} -k_1\left(h_1-h_{1,0}\right)+k_2\left(h_2-h_{2,0}\right)/\alpha_2 \\ -k_2\left(h_2-h_{2,0}\right)+k_3\left(l_3-h_{3,0}\right)/\alpha_3 \\ \vdots \\ -k_{n-2}\left(h_{n-2}-h_{n-2,0}\right)+k_{n-1}\left(h_{n-1}-h_{n-1,0}\right)/\alpha_{n-1} \\ -k_{n-1}\left(h_{n-1}-h_{n-1,0}\right)+k_n\left(h_n-h_{n,0}\right)/\alpha_n \end{bmatrix} \tag{47}$$

$$\boldsymbol{b}^{-}=\begin{bmatrix} k_1\left(h_1-h_{1,0}\right)-\alpha_2 k_2\left(l_2-l_{2,0}\right) \\ k_2\left(h_2-h_{2,0}\right)-\alpha_3 k_3\left(l_3-l_{3,0}\right) \\ \vdots \\ k_{n-2}\left(h_{n-2}-h_{n-2,0}\right)-\alpha_{n-1}k_{n-1}\left(h_{n-1}-h_{n-1,0}\right) \\ k_{n-1}\left(h_{n-1}-h_{n-1,0}\right)-\alpha_n k_n\left(h_n-h_{n,0}\right) \end{bmatrix} \tag{48}$$

where $k_i=EA/h_i$ is the axial stiffness of each segment. With the introduction of the approximation (28), expressions of $\boldsymbol{\varsigma}^{+}$ and $\boldsymbol{\varsigma}^{-}$ can be written as a set of *linear* relationships purely in terms of the unknowns $\boldsymbol{s}$; otherwise a nonlinear relationship will be obtained which will largely complicate the analysis. Substituting Eq. (42) into Eq. (44), we eventually have a standard LCP.

$$\begin{cases} \boldsymbol{w}=\boldsymbol{A}\boldsymbol{z}+\boldsymbol{b} \\ \boldsymbol{0}\le\boldsymbol{w}\perp\boldsymbol{z}\ge\boldsymbol{0} \end{cases} \tag{49}$$

where $\boldsymbol{z}=\begin{bmatrix}\boldsymbol{s}^{+}\\ \boldsymbol{s}^{-}\end{bmatrix}\in\Re^{2(n-1)}$, $\boldsymbol{b}=\begin{bmatrix}\boldsymbol{b}^{+}\\ \boldsymbol{b}^{-}\end{bmatrix}\in\Re^{2(n-1)}$, $\boldsymbol{A}=\begin{bmatrix}\boldsymbol{A}^{+} & -\boldsymbol{A}^{+}\\ -\boldsymbol{A}^{-} & \boldsymbol{A}^{-}\end{bmatrix}\in\Re^{2(n-1)\times 2(n-1)}$.

Problem (49) can be solved by using any available LCP solver. Once a solution $\boldsymbol{z}$ is computed, the sliding magnitude vector $\boldsymbol{s}$ can be obtained by using expression (42). Substituting the sliding magnitude vector $\boldsymbol{s}$ into the expression (31), we complete the calculation of the generalized force vector for the current time step.

Journal Pre-proofs

Importantly, the free length of each segment should be updated by using Eq. (25), in preparation for the analysis of the next time step.

The above calculations are presented in the context of explicit dynamic analyses. Implicit algorithms, such as the Newmark or generalized □□method, can also be adopted for numerical solving of the dynamic governing equation (16). For implicit algorithms, by introducing of a set of linear assumptions (for instance, the Newmark assumptions (Eq. (64))), the dynamic equation can be discretized into a set of nonlinear algebraic equations for the analysis of the current time step. The classical Newton-Raphson scheme is usually applied. In each iteration, the core task is to evaluate two items under the newly updated configuration: (I) the residual generalized force vector and (II) the corresponding Jacobian matrix (tangent matrix). The generalized force vector contributed by the clustered cable element can be obtained in the same manner as in the explicit dynamic analysis presented above. The Jacobian matrix relevant to the clustered cable element is the tangent stiffness matrix, which is commonly computed by taking the derivative of the generalized force vector with respect to the generalized coordinates ($\mathrm{d}\boldsymbol{Q}/\mathrm{d}\boldsymbol{q}$). For a clustered cable element without friction, the tangent stiffness matrix can be rigorously obtained, as did in (Kan et al., 2018c). However, particular challenges arise for the frictional case. Mathematically, to obtain this item one can apply the following chain rule by considering the sliding magnitude vector as an internal variable

$$\frac{\mathrm{d}\boldsymbol{Q}}{\mathrm{d}\boldsymbol{q}}=\frac{\partial \boldsymbol{Q}}{\partial \boldsymbol{q}}+\frac{\partial \boldsymbol{Q}}{\partial \boldsymbol{s}}\frac{\partial \boldsymbol{s}}{\partial \boldsymbol{q}} \tag{50}$$

However, the relationship between the sliding magnitude vector $\boldsymbol{s}$ and the generalized coordinates $\boldsymbol{q}$ is governed by LCP (49) and cannot be expressed by an explicit and smooth function such as $\boldsymbol{s}(\boldsymbol{q})$. In other words, a perturbation of the generalized coordinates may lead to an abrupt change in the sliding magnitude. For conventional implicit dynamic analyses, if a very small time step size is used, the Jacobian matrix is dominated by the mass matrix, and the stiffness matrix of the clustered cables has only a small contribution to the global Jacobian matrix and may be neglected (see, e.g., Eq.(99) in (Kan et al., 2018c)). This operation is, however, limited to an extremely small time step size. For conventional implicit static analyses, the problem becomes even more difficult. When applying the Newton-Raphson scheme in solving the static equilibrium equation (19), one must accurately evaluate the tangent stiffness matrix ($\mathrm{d}\boldsymbol{Q}/\mathrm{d}\boldsymbol{q}$) since this item dominates the global Jacobian matrix. As this item cannot be explicitly expressed, one may use a finite difference approach to obtain the numerical value. This approach, regardless of its inefficiency, cannot guarantee that the iteration is always convergent. During the global Newton-Raphson iteration, the dramatic change of motion states of some connection points will cause a discontinuous change in the tangent stiffness matrix and accordingly may lead to an abrupt change of incremental iterative configuration of two consecutive iterations, and eventually may lead to an oscillation of the solution or to convergence failure. All the aforementioned

numerical difficulties are attributed to the inherent nonsmooth property induced by sliding friction. To alleviate those difficulties in conventional implicit strategies, in the following sections we will present a fully implicit framework based on a nonlinear complementarity function to solve the system static and dynamic equation.

4. Fully implicit static analysis

The core concept of the fully implicit framework in solving the system dynamic or static equilibrium equation is to consider the sliding assistant vector ($s_i^{\pm}$) as additional degrees-of-freedoms, instead of the internal variables, and in combination with the nonlinear complementarity function in the multibody model. We first focus on an implicit static analyses. Extensions to an implicit dynamic analysis will be discussed in the next section.

4.1 Implicit static analysis

According to Section 2.1, by using the original Fischer-Burmeister complementarity function, complementarity relationships (34) can be reformulated as two nonlinear equations.

$$\bar{\psi}_i^{\pm}\left(\varsigma_i^{\pm}, s_i^{\pm}\right) = \sqrt{\left(\varsigma_i^{\pm}\right)^2 + \left(s_i^{\pm}\right)^2} - \left(\varsigma_i^{\pm} + s_i^{\pm}\right) = 0 \tag{51}$$

To increase the stability of the algorithm, the above equations can be further reformulated by considering two aspects.

(I) As pointed noted in Section 2, the Fischer-Burmeister complementarity function is smooth everywhere except at point $(0,0)$. For the current clustered cable problem, the point $\left(\varsigma_i^{\pm}, s_i^{\pm}\right) = (0,0)$ typically corresponds to a state that the connection point is on the verge of sliding, but sliding motion does not truly occur. To resolve the possible numerical difficulty arising from this point, we directly work with a modified Fischer-Burmeister complementarity function $\psi_{\varepsilon}(x,y) = \sqrt{x^2 + y^2 + 2\varepsilon^2} - (x+y)$ (Kanzow, 1996) that possesses the property

$$\psi_{\varepsilon}(x,y) = 0 \Leftrightarrow \left[x \geq 0, y \geq 0, xy = \varepsilon^2\right] \tag{52}$$

where ε is considered as a numerical regularization parameter. Clearly, by using ψ_{ε} the original problem is only solved approximately and becomes sensitive to the choice of the parameter ε. However, according to the author's experience this parameter can be set quite small, e.g., $\varepsilon = 1\times 10^{-14}$, such that the overall effect on the solution is negligible and is close to the usual precision of the numerical procedure itself.

(II) Note that the complementarity variables $\varsigma_i^{\pm}$ possess a unit of force while $s_i^{\pm}$ possess a unit of length. If the SI system is used in real engineering applications, the

value of the tension magnitudes can be very large (such as on the scale of kilonewton) while the value of sliding magnitudes is typically very small (such as on the scale of millimeter), which possibly leads to a numerical ill-condition if Eq. (51) is directly applied. It is thus reasonable from a numerical viewpoint to scale the complementarity variables $\varsigma_i^{\pm}/s_i^{\pm}$ by dividing/multiplying with different large numbers χ_1/χ_2 to balance the order of magnitude differences and improve the stability. The scale factors χ_1 and χ_2 are adjusted heuristically by a prediction of the magnitude of the average tension force and the sliding length.

By applying the above operations, expression (51) can be further reformulated as

$$\psi_i^{\pm}\left(\varsigma_i^{\pm}, s_i^{\pm}\right) = \sqrt{\left(\varsigma_i^{\pm}/\chi_1\right)^2 + \left(\chi_2 s_i^{\pm}\right)^2 + 2\varepsilon^2} - \left(\varsigma_i^{\pm}/\chi_1 + \chi_2 s_i^{\pm}\right) = 0 \tag{53}$$

By defining

$$\boldsymbol{\Psi} = \left[\psi_2^+, \psi_2^-, \psi_3^+, \psi_3^-, ..., \psi_n^+, \psi_n^-\right]^{\mathrm{T}} \in \Re^{2(n-1)} \tag{54}$$

$$\boldsymbol{\varsigma} = \left[\varsigma_2^+, \varsigma_2^-, \varsigma_3^+, \varsigma_3^-, ..., \varsigma_n^+, \varsigma_n^-\right]^{\mathrm{T}} \in \Re^{2(n-1)} \tag{55}$$

$$\overline{\boldsymbol{s}} = \left[s_2^+, s_2^-, s_3^+, s_3^-, ..., s_n^+, s_n^-\right]^{\mathrm{T}} \in \Re^{2(n-1)} \tag{56}$$

and in combination with Eqs. (20)~(27) and (37), we can establish the expression of the complementarity function at the system level, which is a function of both the generalized coordinates ($\boldsymbol{q}$) and the sliding assistant vector ($\overline{\boldsymbol{s}}$).

$$\boldsymbol{\Psi}\left(\boldsymbol{q}, \overline{\boldsymbol{s}}\right) = \boldsymbol{0} \tag{57}$$

It is noteworthy that the above nonlinear complementarity equation is continuous, smooth and differentiable at any point in the domain of definition. The use of the complementarity function is very profound because it allows the transformation of a very complex non-smooth problem into a continuous problem.

The fully implicit static strategy to solve the system can now be formulated. By using Eqs.(38), (39), (42) and (56), we can rewrite the generalized force vector of the clustered cable element (expression (31)) with respect to the sliding assistant vector $\overline{\boldsymbol{s}}$, i.e.,

$$\boldsymbol{Q}_{\mathrm{e}}\left(\boldsymbol{q}, \boldsymbol{s}\right) \to \boldsymbol{Q}_{\mathrm{e}}\left(\boldsymbol{q}, \overline{\boldsymbol{s}}\right) \tag{58}$$

By considering the sliding assistant vector $\overline{\boldsymbol{s}}$ as additional degrees of freedom in combination with the original equilibrium equation (19), the governing equation of the system eventually yields.

$$\boldsymbol{H}\left(\boldsymbol{q}, \boldsymbol{\lambda}, \overline{\boldsymbol{s}}\right) = \begin{bmatrix} \boldsymbol{\Phi}_{\boldsymbol{q}}^{\mathrm{T}}\boldsymbol{\lambda} - \boldsymbol{Q}_{\mathrm{e}}\left(\boldsymbol{q}, \overline{\boldsymbol{s}}\right) \\ \boldsymbol{\Phi}\left(\boldsymbol{q}\right) \\ \boldsymbol{\Psi}\left(\boldsymbol{q}, \overline{\boldsymbol{s}}\right) \end{bmatrix} = \boldsymbol{0} \tag{59}$$

Since the above nonlinear system is continuous, smooth and differentiable everywhere and is complete, the classical Newton-Raphson scheme can be used to

obtain the solution. By defining the unknowns of the system as $\boldsymbol{X}=\left[\boldsymbol{q}^{\mathrm{T}},\boldsymbol{\lambda}^{\mathrm{T}},\bar{\boldsymbol{s}}^{\mathrm{T}}\right]^{\mathrm{T}}$, the standard update relation at the *k*th iteration yields

$$\boldsymbol{X}^{(k+1)}=\boldsymbol{X}^{(k)}+\Delta\boldsymbol{X}^{(k)} \tag{60}$$

where

$$\Delta\boldsymbol{X}^{(k)}=-\left(\frac{\mathrm{d}\boldsymbol{H}}{\mathrm{d}\boldsymbol{X}}\right)^{-1}\boldsymbol{H}\left(\boldsymbol{X}^{(k)}\right) \tag{61}$$

The Jacoboian matrix can be derived as

$$\frac{\mathrm{d}\boldsymbol{H}}{\mathrm{d}\boldsymbol{X}}=\begin{bmatrix}\dfrac{\mathrm{d}\left(\boldsymbol{\Phi}_{\boldsymbol{q}}^{\mathrm{T}}\boldsymbol{\lambda}\right)}{\mathrm{d}\boldsymbol{q}}-\dfrac{\mathrm{d}\boldsymbol{Q}_{\mathrm{e}}}{\mathrm{d}\boldsymbol{q}} & \boldsymbol{\Phi}_{\boldsymbol{q}}^{\mathrm{T}} & -\dfrac{\mathrm{d}\boldsymbol{Q}_{\mathrm{e}}}{\mathrm{d}\bar{\boldsymbol{s}}}\\ \boldsymbol{\Phi}_{\boldsymbol{q}} & \boldsymbol{0} & \boldsymbol{0}\\ \dfrac{\mathrm{d}\boldsymbol{\Psi}}{\mathrm{d}\boldsymbol{q}} & \boldsymbol{0} & \dfrac{\mathrm{d}\boldsymbol{\Psi}}{\mathrm{d}\bar{\boldsymbol{s}}}\end{bmatrix} \tag{62}$$

In the above expression, the four items in the boxes are contributed by the clustered cable element and will be given in the Appendix. The above strategy can be considered as a full coupling strategy where the generalized coordinate ($\boldsymbol{q}$) and the sliding assistant vector ($\bar{\boldsymbol{s}}$) are independent variables. This strategy deals with geometric configuration searching and sliding connection point searching simultaneously. Always the same equation system (59) is solved regardless of whether the motion state of a particular connection point would be sticking or sliding. In other words, any case differentiation of motion state is rigorously avoided which is appealing from an algorithmic point of view.

5. Extension to implicit dynamic analysis

In this section the preceding full implicit strategy will be extended to a dynamic analysis in the context of the classical Newmark algorithm.

The system dynamic equation (16) is a set of highly nonlinear differential-algebraic equations, and the time discretization strategy should be adopted. Let us focus on the analysis of the *n*+1th time step. At the previous *n*th time step, every information is known. By discretizing of Eq. (16) at the *n*+1th time step and in combination with expressions (31) and (58), we have

$$\begin{cases}\boldsymbol{M}_{n+1}\ddot{\boldsymbol{q}}_{n+1}+\boldsymbol{\Phi}_{\boldsymbol{q}_{n+1}}^{\mathrm{T}}\boldsymbol{\lambda}_{n+1}-\boldsymbol{Q}\left(\boldsymbol{q}_{n+1},\dot{\boldsymbol{q}}_{n+1},\bar{\boldsymbol{s}}_{n+1}\right)=\boldsymbol{0}\\ \boldsymbol{\Phi}\left(\boldsymbol{q}_{n+1},t_{n+1}\right)=\boldsymbol{0}\end{cases} \tag{63}$$

where $\boldsymbol{Q}\left(=\boldsymbol{Q}_{\mathrm{e}}-\boldsymbol{Q}_{\mathrm{i}}\right)$ represents the total generalized force vector. The discrete equilibrium equation above is indeterminate since the number of unknowns is greater than that of the equations. The classical Newmark assumption can be introduced

Journal Pre-proofs

$$\begin{cases} \dot{\boldsymbol{q}}_{n+1} = \dot{\boldsymbol{q}}_n + \left[(1-\delta)\ddot{\boldsymbol{q}}_n + \delta\ddot{\boldsymbol{q}}_{n+1}\right]\Delta t \\ \boldsymbol{q}_{n+1} = \boldsymbol{q}_n + \dot{\boldsymbol{q}}_n\Delta t + \left[(1-2\alpha)\ddot{\boldsymbol{q}}_n + 2\alpha\ddot{\boldsymbol{q}}_{n+1}\right]\Delta t^2/2 \end{cases} \tag{64}$$

where Δt is the integration time step, and α and δ are the Newmark parameters. Substituting Eq. (64) into Eq.(63) yields a nonlinear system of the unknowns $\boldsymbol{X}_{n+1} = \left[\boldsymbol{q}_{n+1}^{\mathrm{T}}, \boldsymbol{\lambda}_{n+1}^{\mathrm{T}}, \bar{\boldsymbol{s}}_{n+1}^{\mathrm{T}}\right]^{\mathrm{T}}$, which is still indeterminate due the existence of additional unknowns $\bar{\boldsymbol{s}}_{n+1}$. To complete the task, the nonlinear complementarity equation (57) can be introduced, which eventually yields a set of determinate equations

$$\bar{\boldsymbol{H}}_{n+1}\left(\boldsymbol{q}_{n+1}, \boldsymbol{\lambda}_{n+1}, \bar{\boldsymbol{s}}_{n+1}\right) = \begin{bmatrix} \boldsymbol{M}_{n+1}\ddot{\boldsymbol{q}}_{n+1} + \boldsymbol{\Phi}_{\boldsymbol{q}_{n+1}}^{\mathrm{T}}\boldsymbol{\lambda}_{n+1} - \boldsymbol{Q}_{n+1}\left(\boldsymbol{q}_{n+1}, \dot{\boldsymbol{q}}_{n+1}, \bar{\boldsymbol{s}}_{n+1}\right) \\ \boldsymbol{\Phi}_{n+1}\left(\boldsymbol{q}_{n+1}, t_{n+1}\right) \\ \boldsymbol{\Psi}_{n+1}\left(\boldsymbol{q}_{n+1}, \bar{\boldsymbol{s}}_{n+1}\right) \end{bmatrix} = \boldsymbol{0} \tag{65}$$

The above nonlinear system is continuous, smooth and differentiable everywhere and can be solved by using the classical Newton-Raphson method. The related Jacobian matrix $\mathrm{d}\bar{\boldsymbol{H}}_{n+1}/\mathrm{d}\boldsymbol{X}_{n+1}$ in each iteration is given as

$$\frac{\mathrm{d}\bar{\boldsymbol{H}}_{n+1}}{\mathrm{d}\boldsymbol{X}_{n+1}} = \begin{bmatrix} \dfrac{\boldsymbol{M}_{n+1}}{\alpha\Delta t^2} + \dfrac{\mathrm{d}\left(\boldsymbol{M}_{n+1}\ddot{\boldsymbol{q}}_{n+1}\right)}{\mathrm{d}\boldsymbol{q}_{n+1}} + \dfrac{\mathrm{d}\left(\boldsymbol{\Phi}_{\boldsymbol{q}_{n+1}}^{\mathrm{T}}\boldsymbol{\lambda}_{n+1}\right)}{\mathrm{d}\boldsymbol{q}_{n+1}} - \dfrac{\mathrm{d}\boldsymbol{Q}_{n+1}}{\mathrm{d}\boldsymbol{q}_{n+1}} - \dfrac{\delta}{\alpha\Delta t}\dfrac{\mathrm{d}\boldsymbol{Q}_{n+1}}{\mathrm{d}\dot{\boldsymbol{q}}_{n+1}} & \boldsymbol{\Phi}_{\boldsymbol{q}_{n+1}}^{\mathrm{T}} & -\dfrac{\mathrm{d}\boldsymbol{Q}_{n+1}}{\mathrm{d}\bar{\boldsymbol{s}}_{n+1}} \\ \boldsymbol{\Phi}_{\boldsymbol{q}_{n+1}} & \boldsymbol{0} & \boldsymbol{0} \\ \dfrac{\mathrm{d}\boldsymbol{\Psi}_{n+1}}{\mathrm{d}\boldsymbol{q}_{n+1}} & \boldsymbol{0} & \dfrac{\mathrm{d}\boldsymbol{\Psi}_{n+1}}{\mathrm{d}\bar{\boldsymbol{s}}_{n+1}} \end{bmatrix} \tag{66}$$

Similar to the static case, the four items in the boxes are contributed by the clustered cable element and can be computed by taking advantage of the expressions presented in the Appendix. Once the solution $\boldsymbol{X}_{n+1}$ is found the generalized velocity vector and generalized acceleration vector can be determined by using the Newmark assumption (64). This completes the analysis of the current time step.

6. Numerical examples

Two numerical examples are presented in this section to illustrate the performance the proposed framework as well as to reveal some novel phenomena involved in clustered cable analysis when considering friction.

6.1 A strut moving on a clustered cable

The first example is a simple example that involves static analyses of a strut moving on a clustered cable. Similar systems were investigated in (Wu et al., 2019; Zhou et al., 2004) using a finite element formulation, and friction was not considered. For such a system, the system configuration at some limit states can be obtained through an

analytical manner so that the numerical results obtained by the proposed approach can be validated. As shown in Fig. 11 (a), a rigid bar-like strut with its one end being subjected to a concentrated force F of which the magnitude is a constant while the direction is variable. A small pulley is installed at the other end of the strut and can slide along the clustered cable with friction. The clustered cable is assumed undamped, weightless and inextensible. At the initial state, the direction of the applied force is vertical and upward ($\varphi = 0$). The system is in equilibrium, and the two segments of the clustered cable are balanced and possess the same tension magnitudes. We are interested in how the system evolves when the force direction φ quasi-statically varies from 0 to 90°. The parameters of the system are considered dimensionless, with values of F = 100, $l = d$ = 1, θ_0=45°. The strut is modeled as a rigid body. An elastic linear constitutive relation is chosen for the cable segments with a high Young's modulus to mimic the inextensibility of the cable. Different cases of friction coefficient are considered: μ = 0, 0.2, 0.5 and 1.

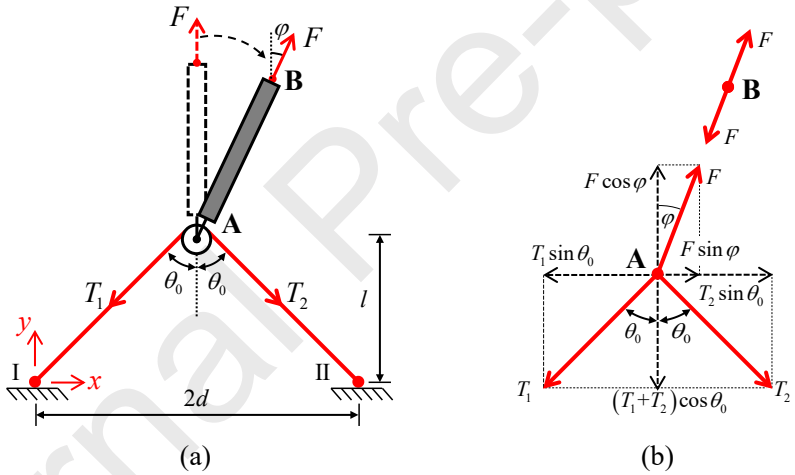


Fig. 11 (a) A strut moving on a clustered cable; (b) force analysis at the limit equilibrium state.

The problem is solved using the fully implicit static approach proposed in Section 4 with a multistep loading strategy (200 loading steps in total). In the nonlinear complementarity equation (53), the numerical regularization parameter is chosen as $\varepsilon = 1\times10^{-14}$, and the scaling factors are chosen as $\chi_1 = \chi_2 = 1\times10^{3}$ based on a prediction of the order of the tension magnitude and the sliding magnitude. The convergence tolerance for the Newton-Raphson scheme is set to $\xi = 1\times10^{-7}$.

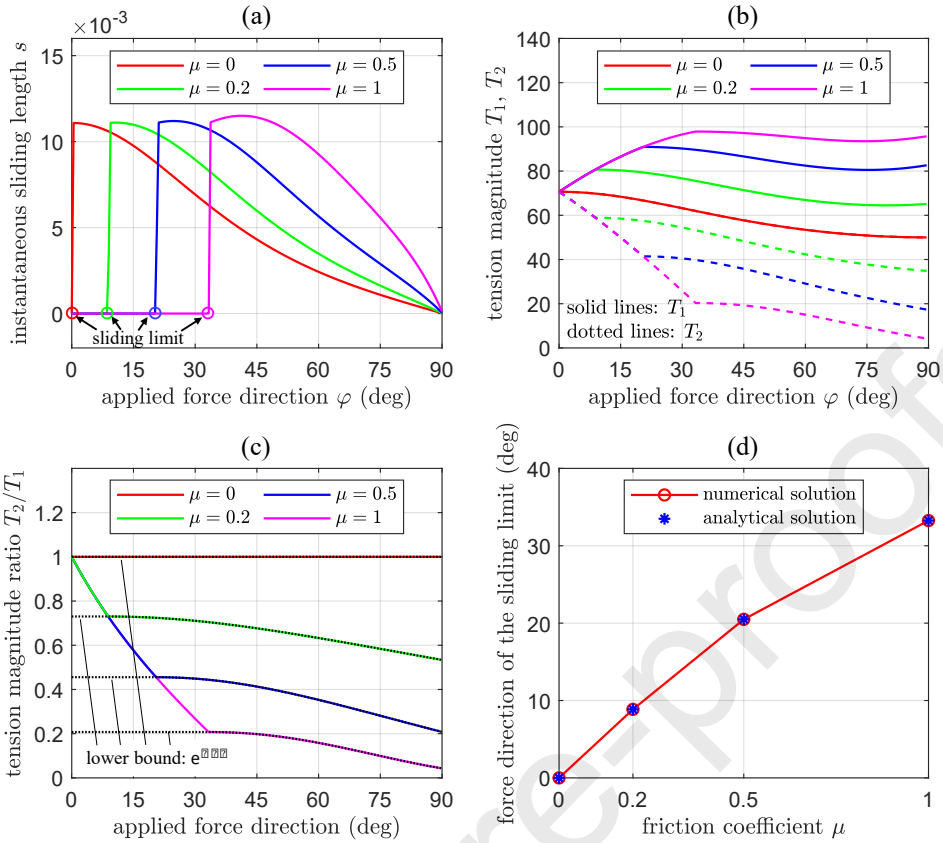


Fig. 12 Curves of some numerical results with the evolution of the applied force direction: (a) instantaneous sliding length, (b) tension magnitudes, (c) tension magnitude ratio. (d) Comparison of the force direction between the numerical and analytical solutions.

Fig. 12 (a)-(c) presents the curves of instantaneous sliding length, tension magnitudes and tension magnitude ratio, with the evolution of the applied force direction. The results show that friction has a significant influence on the system mechanical response. For the frictionless case ($\mu = 0$), once the force direction begins to change, the connection point immediately and continuously slides to end point II ($s > 0$), and the tension magnitudes of the two segments are exactly the same. For the frictional cases, the motion state of the connection point is slightly complex. At the beginning, the connection point is in a sticking state ($s = 0$), and the tension magnitude ratio decreases until a sliding limit state is achieved. In such a state, the tension magnitude ratio is exactly located at the ‘‘lower bound” defined by the sliding criterion. Then, the connection point begins to continuously slide, and the tension magnitude ratio remains at the ‘‘lower bound”, which is not a constant due to the variation of the contact angle. These outcomes agree perfectly with the modeling assumptions and the sliding criterion. Fig. 13 presents some system equilibrium configurations with the evolution of the applied force direction for two representative friction coefficients. The sticking and sliding motion states of the connection point for the frictional case can be clearly observed. Due to the force equilibrium, the strut orientation and the applied force direction are always accordant. In addition, it is interesting to find that the trajectory of

the connection point depicts an elliptical arc, which is self-evident according to the first definition of an ellipse.

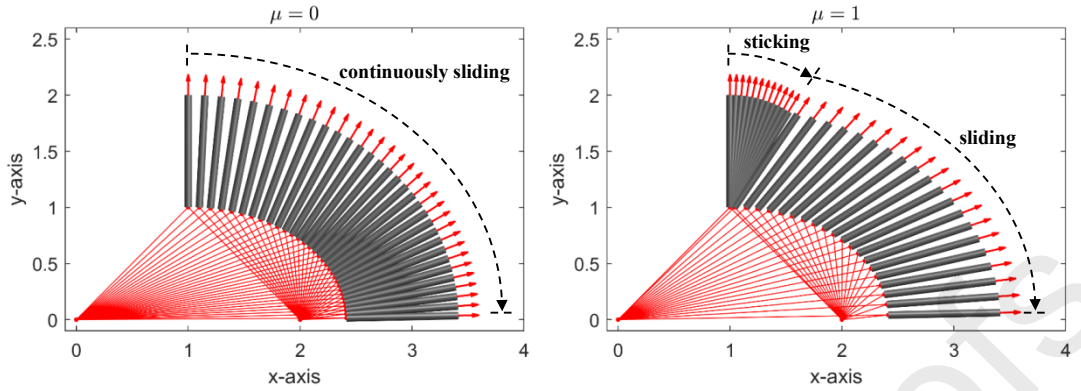


Fig. 13 Some system equilibrium configurations with the evolution of the applied force direction.

To quantitatively verify the numerical results, we obtain the analytical solutions of the force direction corresponding to the sliding limit state by using the limit equilibrium equation (as illustrated in Fig. 11 (b))

$$\begin{cases} T_1 \sin\theta_0 - T_2 \sin\theta_0 = F \sin\varphi \\ T_1 \cos\theta_0 + T_2 \cos\theta_0 = F \cos\varphi \\ T_1 = T_2 \mathrm{e}^{\mu(\pi - 2\theta_0)} \end{cases} \tag{67}$$

As shown in Fig. 12 (d), the numerical solutions for all friction coefficients agree perfectly with the analytical solutions, which demonstrates the correctness of the proposed approach. In addition, it is noteworthy that the limit equilibrium equation (67) can only be given when the tendency of the sliding direction is known or can be easily guessed. For a complex system, we by no means know in advance the motion states of the connection points and therefore cannot formulate such kind of equation in general. This represents the inherent difficulties in solving clustered cable problems. The principles of the proposed approach as well as its implementation are validated against this simple sliding mechanism, showing that the above difficulties can be automatically handled in a unified, continuous and smooth manner. Complex tensegrity systems involving clustered cable elements can now be studied.

6.2 Mechanical bending analyses of a tensegrity spine

In recent years, the tensegrity concept has been used in many engineering fields due to its unique structural properties. In particular, in bioengineering, the tensegrity concept has been recognized as a simple and effective model to reproduces the mechanics of some complicated biological units such as spines (Brian R. Tietz et al., 2013; Kardas et al., 2013) and cells (Ingber, 2003a, b). While most of the literature in bioengineering involving tensegrity usually focuses on a concept description, specific quantitative analysis seems rarely seen. In this subsection, we investigate the mechanical bending responses of a tensegrity spine. Both static and dynamic analyses will be involved. The aim is, on one hand, to demonstrate the proposed framework in a more complex system and, on the other hand to make an attempt to develop some basic

impression into the mechanical properties of such a structure, which may benefit its specific application.

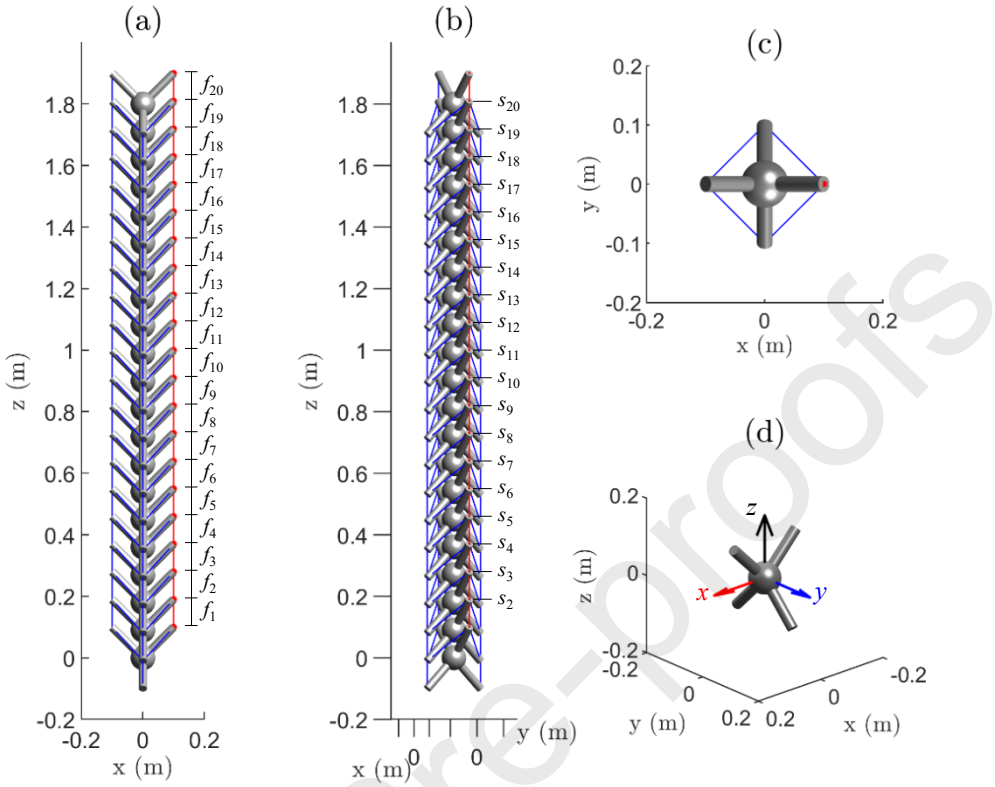


Fig. 14 System configuration of the tensegrity spine at the initial state: (a) a side view, (b) a perspective view, (c) a top view. (d) A particular strut and the local fixed coordinate frame.

We consider a beam-like tensegrity spine shown in Fig. 14, where the grey objects denote struts, the blue lines denote classical cables and the red line denote a clustered cable. The system is assembled by twenty-one in-line identical struts. The struts are isolated and connected only by cables from each other, making the system a class 1 tensegrity structure. To easily actuate the structure, one side of the vertical cables is replaced by a clustered cable, and the others remain as classical cables. The clustered cable contains twenty segments and twenty-one connection points with the struts. Particular features of this kind of structure are that the struts are of complex shapes, rather conventionally "thin and long", and a particular strut may connect to the cables with multiple points, rather than with only the "two ends". These features make it difficult to use the conventional finite element approach to effectively handle the mechanical response analysis, as has been illustrated in the introduction. The proposed multibody-based modeling method is thus used. The struts are modeled as rigid bodes with local coordinate frames located at the respective mass centers and the frame directions are parallel to the inertial principal axis (shown in Fig. 14 (d)). The mass of a strut is taken as $m = 0.2$ kg, and the inertia tensor is taken as $\boldsymbol{J}' = \mathrm{diag}\left[5.27,\ 5.27,\ 3.81\right]\times 10^{-4}\ \mathrm{kg\bullet m^2}$, which is obtained by fully taking into account the geometric shape and the density of the strut. The structure has an overall height of

2 m, a width and a length of 0.2 m. Other material and dimensional parameters are presented in **Table 1**.

Table 1 Detailed material and dimensional parameters of the tensegrity spine.

Parameter	Value
Young's modulus of all the cables (GPa)	110
Initial length of each segment of the clustered cable (cm)	9
Initial length of the vertical classical cables (cm)	9
Initial length of the oblique classical cables (cm)	17.92
Diameter of the vertical classical cables (mm)	0.05
Diameter of the oblique classical cables (mm)	0.2
Diameter of the clustered cable (mm)	1
Prestress force in the vertical classical cables (N)	1000
Prestress force in the oblique classical cables (N)	1628.58
Prestress force in each segment of the clustered cable (N)	1000

At the initial state, the structure is in a straight shape. Prestress forces are introduced in the structure to eliminate possible infinitesimal mechanisms (Calladine and Pellegrino, 1991) and provide the necessary structural stiffness. The bottom strut is fixed on the space as a boundary condition. The actuated bending deformation of the structure is emphatically studied. Bending deformation is achieved via an actuation of the clustered cable, in such a way that the free length of the first (bottom) segment of the clustered cable is progressively shortened. This strategy is equivalent to stretching the one end of the clustered cable, as in (Kan et al., 2018c). The actuation will not terminate until a designated maximum actuation value (v) is achieved.

We first study the system general bending behavior quasi-statically. It is assumed that the actuation speed of the clustered cable is extremely low such that the inertial effects can be negligible. To investigate the influence of friction on the structural behavior, varying values of the friction coefficient are performed: μ = 0, 0.005, 0.01, and 0.02. The analyses are conducted using the implicit static nonlinear complementarity function based approach proposed in Section 4 with a multistep loading strategy (250 loading steps in total). The maximum actuation value is taken as v = 0.5 m. For bending deformations, the contact angles related to the connection points evolve minimally and thus are considered constants equal to 2π. The numerical regularization parameter in the nonlinear complementarity equation (53) is chosen as $\varepsilon = 1\times10^{-14}$. The scaling factors are chosen as $\chi_1 = \chi_2 = 1\times10^{3}$. The convergence tolerance for the Newton-Raphson scheme is set to $\xi = 1\times10^{-7}$.

Journal Pre-proofs

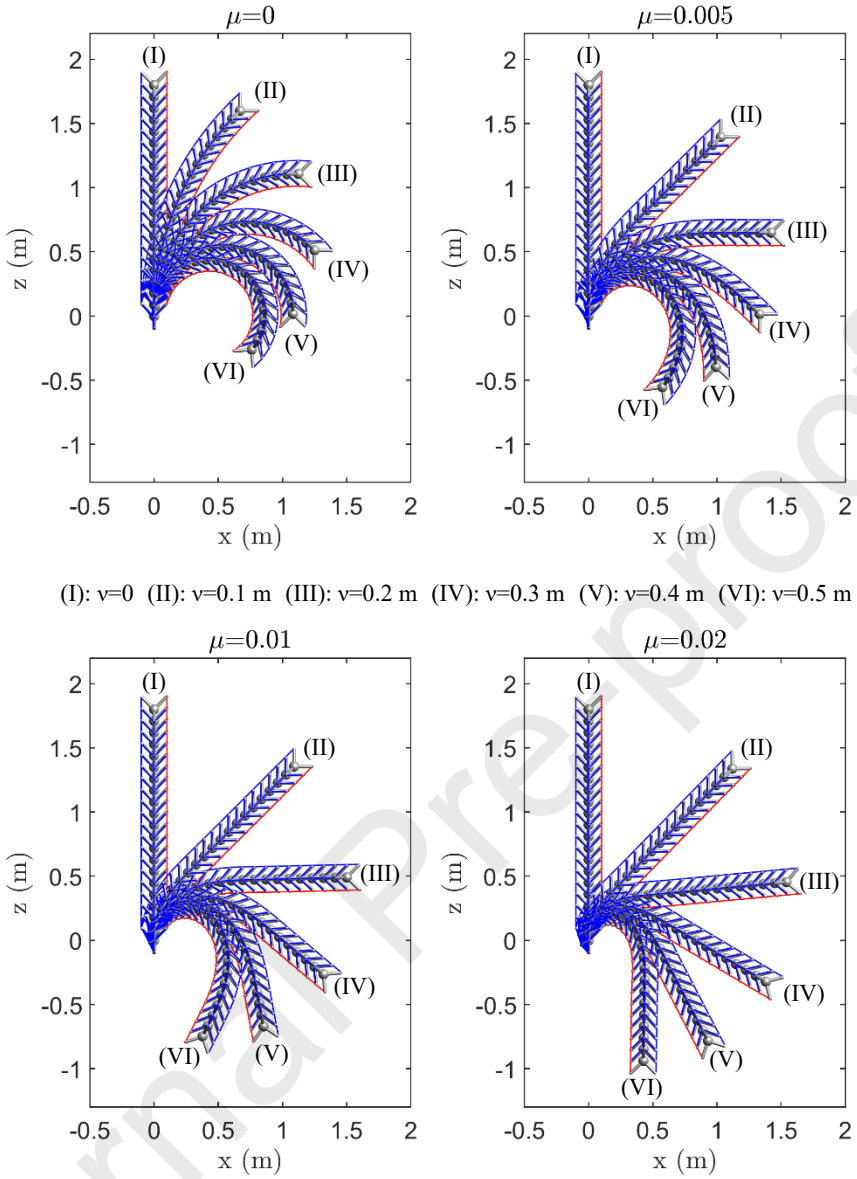


Fig. 15 The deformed configurations under some representative actuation values for different friction coefficients.

Fig. 15 shows the deformed configurations of the structure under some representative actuation values. It is clear that with the actuation being performed, the structure can be successfully bent. However, it can also be observed that the friction coefficient has a great influence on the bending deformation. For the frictionless case ($\mu = 0$), the structure is bent with an equal bending curvature from the bottom to the top of the structure, and therefore appears as an arc shape. For the three frictional cases, the deformed configurations are much different. For the small friction coefficient (μ = 0.005), the bottom of the structure is first bent, and the top of the structure remains straight until a large actuation value has been achieved. For the relatively large friction coefficients considered (μ = 0.01 and 0.02), the bottom of the structure is bent, while

Journal Pre-proofs

the top still maintains straight even if the maximum actuation value is achieved. To gain insight, Fig. 16 presents the tension magnitude curves of each segment of the clustered cable. Fig. 17 gives the instantaneous sliding length curves of the connection points. For the frictionless case, it is expected that the tension magnitudes of all the segments are identically and monotonically increasing. All the connection points continuously slide from beginning to end. For a small friction coefficient case ($\mu = 0.005$), the tension magnitude in the bottom segment first increases, and that in the top segments remains unchanged. Tension difference occurs. When the difference "exceeds" the sliding limit, sliding motion occurs and the tensions are balanced to meet the limit state. From Fig. 17, it is interesting to find that these connection points slide in a unified direction from the bottom end to the top end one by one. This eventually leads to a situation in which the tension magnitudes in the clustered cable decay strictly from the bottom end to the top end according to the sliding criterion (33). For the largest friction coefficient case ($\mu = 0.02$), those connection points close to the top end of the structure remain stick even if the maximum actuation value is achieved. A large tension difference occurs in this case: the maximal tension magnitude is as high as four times the minimal tension magnitude. To summarize, the numerical results are very sensitive to the friction coefficient, and the results highlight the complex mechanical behavior, in particular the tension difference and the asynchronicity for the sliding behavior of the connection points.

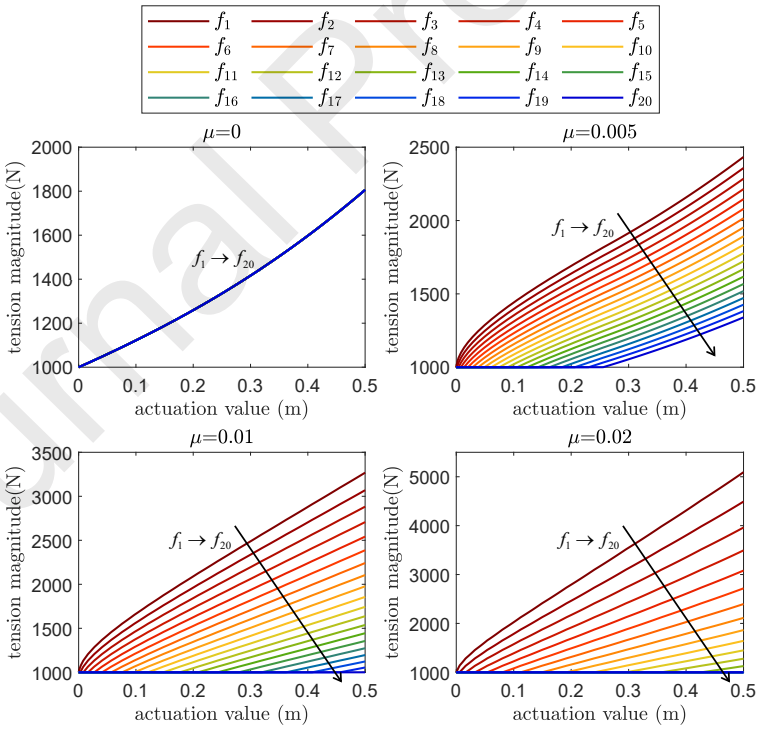


Fig. 16 The tension magnitude curves of each segment of the clustered cable with the evolution of the actuation value.

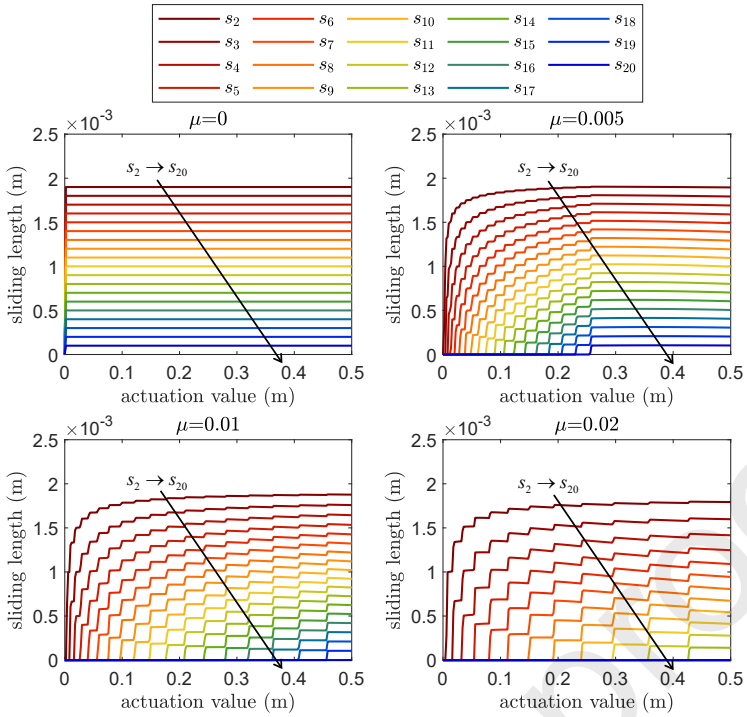


Fig. 17 The instantaneous sliding length curves of the connection points with the evolution of the actuation value.

Next, we consider a dynamic actuation strategy, which assumes that the first segment of the clustered cable is progressively shortened with a certain speed V. As indicated in Fig. 18, the actuation speed considered here is time-varying with a maximum value of 0.1 m/s. A topic of our future work is to couple the control algorithm (Peng et al., 2020) to design an optimal motion speed. The total simulation time is set as 10 s, where the time interval exceeds the actuation time aims to observe the vibration characteristics of the system. To avoid an excessive tension magnitude difference, we use a relatively small friction coefficient μ= 0.01. The dynamic analysis is performed by using the implicit complementarity function based approach proposed in Section 5, with the Newmark parameters being chosen as $\alpha = 0.3$, $\delta = 0.5$, and the time step size is taken as $\Delta t = 2\times 10^{-4}$ s.

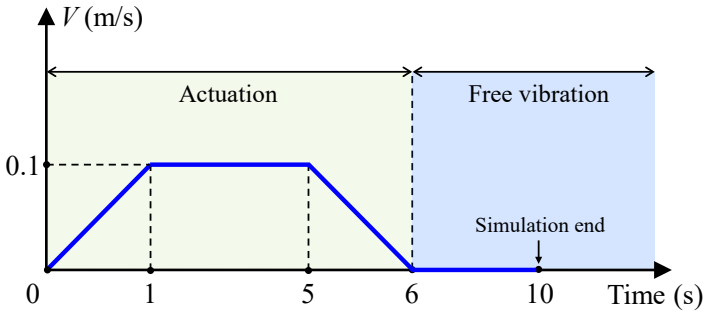


Fig. 18 The time-varying actuation speed.

Fig. 19 shows the time history curves of the tension magnitude of all segments of

the clustered cable. Generally, in the actuation phase (0~6 s) the evolution of the tension magnitudes is similar to that of the static case presented in Fig. 16. With the actuation being performed, the tension magnitudes of almost all the segments increase. The tension magnitude of the last segment remains almost invariable, which can be attributed to the fact that for the current friction coefficient the maximum actuation value is insufficient to yield a real sliding motion for the last possible connection point. The closer the segments to the bottom end, the larger the tension magnitudes. However, given the complex dynamic effects, the tension magnitudes do not strictly monotonously increase with the segment indices. In the free vibration phase (6~10 s), it is expected that all the tension magnitude curves vibrate with different amplitudes.

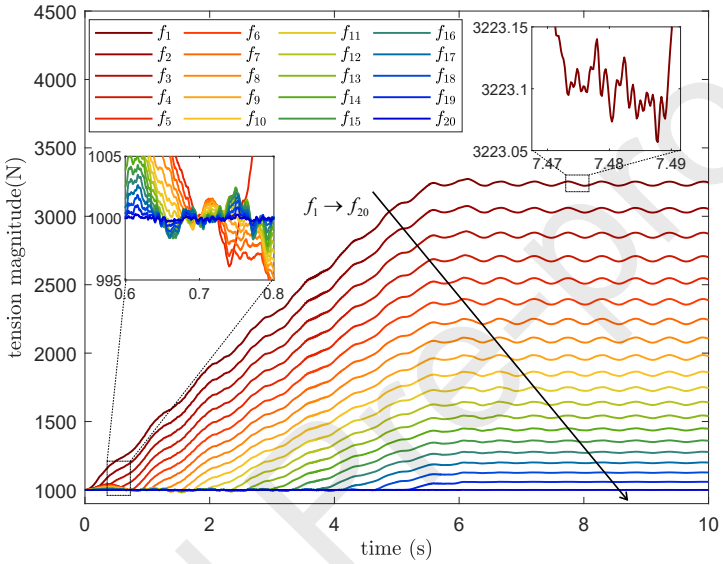


Fig. 19 The time history curves of the tension magnitude of all segments of the clustered cable.

To further demonstrate the complex interactive coupling mechanism between the dynamic effects and the friction. Fig. 20 and Fig. 21 present comparisons between the time history curve of the tension magnitude ratio and that of the instantaneous sliding length relevant to the 2nd and 18th connection points, respectively. It can be seen that for the dynamic actuation strategy, the motion behavior of the connection points is very complex. In particular, in the free vibration phase (6~10 s), the connection points mainly exist in a sticking state, while accidental sliding motions can occur. The solutions demonstrate that for all the positive sliding lengths the relevant tension magnitude ratios are exactly located at the lower bound defined by the sliding criterion, while for all the instantaneous sliding lengths of zero the relevant tension magnitude ratios are located upon the lower bound. These results agree perfectly with the sliding criterion (33), which from a side view illustrates the correctness of the numerical solutions. To summarize, this example highlights the influence of friction on the general mechanical behavior of the system, and reveals the complex and diverse motion states of the connection points, particularly the stick-slip phenomenon involved. To accurately analyze this kind of system, friction must be taken into account, which can be effectively and robustly handled by using the methodology developed.

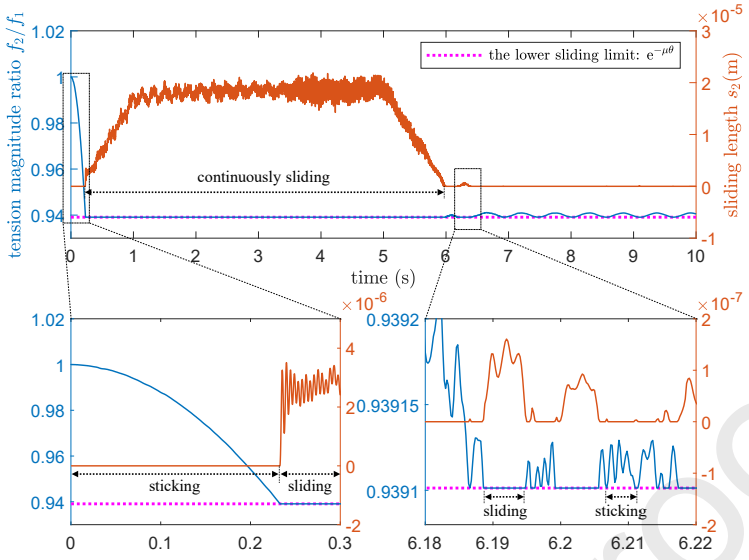


Fig. 20 Comparisons between the time history curve of the tension magnitude ratio and that of the instantaneous sliding length relevant to the 2nd connection point (s_2).

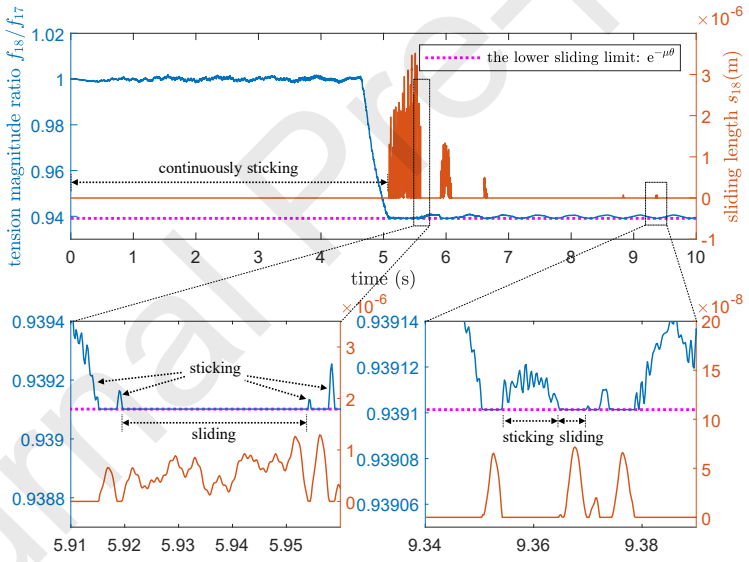


Fig. 21 Comparisons between the time history curve of the tension magnitude ratio and that of the instantaneous sliding length relevant to the 18th connection point (s_{18}).

7. Conclusions

Structures with clustered cables are widespread in many engineering applications. Most of the works in the existing literature involving clustered cables are based on the finite element approach. This paper presents a different multibody-based framework for the mechanical analysis of clustered cable systems. The generalized coordinates of the system are chosen as the configurations of the attached rigid bodies, rather than traditional nodal displacements or positions in the finite element formulation. To address friction induced by cable sliding, we propose a comprehensive

Journal Pre-proofs

complementarity-based framework. For explicit dynamic analyses, a non-smooth LCP approach is proposed. At a particular time step, the determination of the motion states of the possible sliding points is formulated as a standard linear complementarity formulation that can be solved by applying any available mature LCP solvers. For implicit static and dynamic analyses, the challenging problem is that both the system deformed configuration and the motion states of the possible sliding points are unknown for a particular loading/time step. We develop a nonlinear complementarity function based approach to address this problem, which allows us to solve the problem in a unified, continuous and smooth manner. The solution can be obtained by using the classical Newton-Raphson method with a closed-form expression of the Jacobian matrix. The great advantage is that any case differentiation for the sudden motion state change of the connection points is rigorously avoided, and the same equation is always used, which is appealing from an algorithm implementation point of view.

As a representative engineering application, the developed framework is employed in mechanical analyses of active tensegrity structures. The struts in the system are modeled as rigid bodies and the cables are considered as internal force elements acting on those rigid bodies. The large overall motions of struts are described by the local fixed frames. In contrast to the finite element formulation, this modeling method is especially adapted for analyzing tensegrity structures with struts of arbitrary shape and with any number of connection points between a particular strut and the cables. The numerical results show that the friction between the clustered cable and the struts fundamentally alters the system mechanical behavior. For static analyses, it is emphasized that friction leads to significant differences in tension magnitude for different segments of a clustered cable. For dynamic analyses, the results reveal that novel behavior, such as the stick-slip phenomenon of the connection points, can occur frequently. The outcomes demonstrate the ability of the proposed methodology to capture the complex and diverse motion states.

Acknowledgments

The authors are grateful for the financial support of the National Key Research and Development Plan (2019YFB1706502); the National Natural Science Foundation of China (12002072,11922203).

Appendix

A. Definition of the derivative of a vector

If $\boldsymbol{y}$ is an m-dimensional column vector, i.e., $\boldsymbol{y}=\left[y_1, y_2, \cdots, y_m\right]^{\mathrm{T}}$, and $\boldsymbol{x}$ is an n-dimensional column vector, i.e., $\boldsymbol{x}=\left[x_1, x_2, \cdots, x_n\right]^{\mathrm{T}}$, the derivative of the vector $\boldsymbol{y}$ with respect to the vector $\boldsymbol{x}$ is given as :

$$\frac{\partial \boldsymbol{y}}{\partial \boldsymbol{x}}=\begin{bmatrix} \frac{\partial y_1}{\partial x_1} & \cdots & \frac{\partial y_1}{\partial x_n} \\ \vdots & \ddots & \vdots \\ \frac{\partial y_m}{\partial x_1} & \cdots & \frac{\partial y_m}{\partial x_n} \end{bmatrix} \in \Re^{m\times n} \tag{68}$$

B. The tangent matrices

In this Appendix, we will present detailed expressions of the tangent matrices contributed by the clustered cable element. As indicated in Eq.(62), the expressions contains four parts: $\mathrm{d}\boldsymbol{Q}_{\mathrm{e}}/\mathrm{d}\boldsymbol{q}$, $\mathrm{d}\boldsymbol{Q}_{\mathrm{e}}/\mathrm{d}\overline{\boldsymbol{s}}$, $\mathrm{d}\boldsymbol{\Psi}/\mathrm{d}\boldsymbol{q}$ and $\mathrm{d}\boldsymbol{\Psi}/\mathrm{d}\overline{\boldsymbol{s}}$.

B.1 The first part $\mathrm{d}\boldsymbol{Q}_{\mathrm{e}}/\mathrm{d}\boldsymbol{q}$

To obtain this item, we first focus on a particular segment. For the *i*th segment of the clustered cable, taking the partial derivatives of some key terms with respect to the associated generalized coordinate ($\boldsymbol{q}_p$ and $\boldsymbol{q}_q$), we have

$$\frac{\partial h_i}{\partial \boldsymbol{q}_p}=\frac{\boldsymbol{h}_i^{\mathrm{T}}}{h_i}\frac{\partial \boldsymbol{h}_i}{\partial \boldsymbol{q}_p}=\hat{\boldsymbol{h}}_i^{\mathrm{T}}\boldsymbol{B}_i;\ \frac{\partial h_i}{\partial \boldsymbol{q}_q}=\frac{\boldsymbol{h}_i^{\mathrm{T}}}{h_i}\frac{\partial \boldsymbol{h}_i}{\partial \boldsymbol{q}_q}=-\hat{\boldsymbol{h}}_i^{\mathrm{T}}\boldsymbol{B}_{i+1} \tag{69}$$

$$\frac{\partial \hat{\boldsymbol{h}}_i}{\partial \boldsymbol{q}_p}=\frac{1}{h_i}\left(\boldsymbol{I}_3-\hat{\boldsymbol{h}}_i\hat{\boldsymbol{h}}_i^{\mathrm{T}}\right)\boldsymbol{B}_i;\ \frac{\partial \hat{\boldsymbol{h}}_i}{\partial \boldsymbol{q}_q}=-\frac{1}{h_i}\left(\boldsymbol{I}_3-\hat{\boldsymbol{h}}_i\hat{\boldsymbol{h}}_i^{\mathrm{T}}\right)\boldsymbol{B}_{i+1} \tag{70}$$

By taking the partial derivatives of the tension magnitude (F_i) with respect to the associated generalized coordinate ($\boldsymbol{q}_p$ and $\boldsymbol{q}_q$), and using expressions (22), (25)~(27), and (69) we have

$$\frac{\partial F_i}{\partial \boldsymbol{q}_p}=\frac{EA}{h_{i,\mathrm{f}}}\frac{\partial h_i}{\partial \boldsymbol{q}_p}=\frac{EA\hat{\boldsymbol{h}}_i^{\mathrm{T}}\boldsymbol{B}_i}{h_{i,\mathrm{f}}}\ ;\ \frac{\partial F_i}{\partial \boldsymbol{q}_q}=\frac{EA}{h_{i,\mathrm{f}}}\frac{\partial h_i}{\partial \boldsymbol{q}_q}=-\frac{EA\hat{\boldsymbol{h}}_i^{\mathrm{T}}\boldsymbol{B}_{i+1}}{h_{i,\mathrm{f}}} \tag{71}$$

It can be noted from Eq. (14) that matrix $\boldsymbol{B}_i$ is a function only of $\boldsymbol{q}_p$ and $\boldsymbol{u}_i$, and matrix $\boldsymbol{B}_{i+1}$ is a function only of $\boldsymbol{q}_q$ and $\boldsymbol{u}_{i+1}$, which implies that

$$\frac{\partial\left(\boldsymbol{B}_i^{\mathrm{T}}\boldsymbol{V}_3\right)}{\partial \boldsymbol{q}_q}=\left[\boldsymbol{0}\right]_{6\times 6}\ ;\ \frac{\partial\left(\boldsymbol{B}_{i+1}^{\mathrm{T}}\boldsymbol{V}_3\right)}{\partial \boldsymbol{q}_p}=\left[\boldsymbol{0}\right]_{6\times 6} \tag{72}$$

where $\boldsymbol{V}_n$ denotes an arbitrary *n*-dimensional column vector. As a result, we have

Journal Pre-proofs

$$\begin{cases} \dfrac{\partial\left(\boldsymbol{B}_i^{\mathrm{T}}\hat{\boldsymbol{h}}_i\right)}{\partial \boldsymbol{q}_p}=\boldsymbol{B}_i^{\mathrm{T}}\dfrac{\partial \hat{\boldsymbol{h}}_i}{\partial \boldsymbol{q}_p}+\left.\dfrac{\partial\left(\boldsymbol{B}_i^{\mathrm{T}}\boldsymbol{V}_3\right)}{\partial \boldsymbol{q}_p}\right|_{\boldsymbol{V}_3=\hat{\boldsymbol{h}}} \quad ; \quad \dfrac{\partial\left(\boldsymbol{B}_i^{\mathrm{T}}\hat{\boldsymbol{h}}_i\right)}{\partial \boldsymbol{q}_q}=\boldsymbol{B}_i^{\mathrm{T}}\dfrac{\partial \hat{\boldsymbol{h}}_i}{\partial \boldsymbol{q}_q} \\ \dfrac{\partial\left(\boldsymbol{B}_{i+1}^{\mathrm{T}}\hat{\boldsymbol{h}}_i\right)}{\partial \boldsymbol{q}_q}=\boldsymbol{B}_{i+1}^{\mathrm{T}}\dfrac{\partial \hat{\boldsymbol{h}}_i}{\partial \boldsymbol{q}_q}+\left.\dfrac{\partial\left(\boldsymbol{B}_{i+1}^{\mathrm{T}}\boldsymbol{V}_3\right)}{\partial \boldsymbol{q}_q}\right|_{\boldsymbol{V}_3=\hat{\boldsymbol{h}}} \quad ; \quad \dfrac{\partial\left(\boldsymbol{B}_{i+1}^{\mathrm{T}}\hat{\boldsymbol{h}}_i\right)}{\partial \boldsymbol{q}_p}=\boldsymbol{B}_{i+1}^{\mathrm{T}}\dfrac{\partial \hat{\boldsymbol{h}}_i}{\partial \boldsymbol{q}_p} \end{cases} \tag{73}$$

Taking the derivatives of Eq. (30) with respect to the associated generalized coordinate ($\boldsymbol{q}_p$ and $\boldsymbol{q}_q$), we have

$$\begin{cases} \dfrac{\mathrm{d}\boldsymbol{Q}_p^{(i)}}{\mathrm{d}\boldsymbol{q}_p}=-F_i\dfrac{\partial\left(\boldsymbol{B}_i^{\mathrm{T}}\hat{\boldsymbol{h}}_i\right)}{\partial \boldsymbol{q}_p}-\boldsymbol{B}_i^{\mathrm{T}}\hat{\boldsymbol{h}}_i\dfrac{\partial F_i}{\partial \boldsymbol{q}_p} \quad ; \quad \dfrac{\mathrm{d}\boldsymbol{Q}_p^{(i)}}{\partial \boldsymbol{q}_q}=-F_i\dfrac{\partial\left(\boldsymbol{B}_i^{\mathrm{T}}\hat{\boldsymbol{h}}_i\right)}{\partial \boldsymbol{q}_q}-\boldsymbol{B}_i^{\mathrm{T}}\hat{\boldsymbol{h}}_i\dfrac{\partial F_i}{\partial \boldsymbol{q}_q} \\ \dfrac{\mathrm{d}\boldsymbol{Q}_q^{(i)}}{\mathrm{d}\boldsymbol{q}_p}=F_i\dfrac{\partial\left(\boldsymbol{B}_{i+1}^{\mathrm{T}}\hat{\boldsymbol{h}}_i\right)}{\partial \boldsymbol{q}_p}+\boldsymbol{B}_{i+1}^{\mathrm{T}}\hat{\boldsymbol{h}}_i\dfrac{\partial F_i}{\partial \boldsymbol{q}_p} \quad ; \quad \dfrac{\mathrm{d}\boldsymbol{Q}_q^{(i)}}{\mathrm{d}\boldsymbol{q}_q}=F_i\dfrac{\partial\left(\boldsymbol{B}_{i+1}^{\mathrm{T}}\hat{\boldsymbol{h}}_i\right)}{\partial \boldsymbol{q}_q}+\boldsymbol{B}_{i+1}^{\mathrm{T}}\hat{\boldsymbol{h}}_i\dfrac{\partial F_i}{\partial \boldsymbol{q}_q} \end{cases} \tag{74}$$

Substituting Eqs. (71) and (73) into Eq. (74) yields the final expression of the tangent matrix of the first part at the segment level. By assembling expression (74) into a system level using the mapping matrix $\boldsymbol{C}_i$ and using Eq. (31), we eventually derive the expression of the tangent matrix of the first part, which yields

$$\frac{\mathrm{d}\boldsymbol{Q}_{\mathrm{e}}}{\mathrm{d}\boldsymbol{q}}=\sum_{i=1}^{n}\left(\boldsymbol{C}_i\otimes\boldsymbol{I}_6\right)^{\mathrm{T}}\begin{bmatrix}\dfrac{\mathrm{d}\boldsymbol{Q}_p^{(i)}}{\mathrm{d}\boldsymbol{q}_p} & \dfrac{\mathrm{d}\boldsymbol{Q}_p^{(i)}}{\mathrm{d}\boldsymbol{q}_q}\\ \dfrac{\mathrm{d}\boldsymbol{Q}_p^{(i)}}{\mathrm{d}\boldsymbol{q}_p} & \dfrac{\mathrm{d}\boldsymbol{Q}_p^{(i)}}{\mathrm{d}\boldsymbol{q}_q}\end{bmatrix}\left(\boldsymbol{C}_i\otimes\boldsymbol{I}_6\right) \tag{75}$$

It can be found that to obtain the exact tangent matrix, one should also evaluate some terms (matrices) such as $\partial\left(\boldsymbol{B}_i^{\mathrm{T}}\boldsymbol{V}_3\right)/\partial\boldsymbol{q}_p$. Theoretically, these terms can be written in a form of a third-order tensor by multiplying the corresponding vector. However, this operation is complex and not conducive to numerical implementations. To simplify the numerical calculation, the detailed expressions of such term is given in Appendix C.

B.2 The second part $\mathrm{d}\boldsymbol{Q}_{\mathrm{e}}/\mathrm{d}\overline{\boldsymbol{s}}$

First, it should be noted that the tension magnitude of the *i*th segment (F_i) is a function only of the sliding magnitude of the points it connects to (s_i and s_{i+1}) and is independent of the other sliding magnitudes. By defining a matrix $\overline{\boldsymbol{C}}\in\Re^{n\times(n-1)}$,

Journal Pre-proofs

$$\bar{\boldsymbol{C}}=\begin{bmatrix}1 & & & \\ -1 & 1 & & \\ & \ddots & \ddots & \\ & & -1 & 1 \\ & & & -1\end{bmatrix} \tag{76}$$

it can be verified from Eqs. (25)~(27) that the following relationship holds

$$\frac{\partial F_i}{\partial \boldsymbol{s}}=\frac{EAh_i}{h_{i,\mathrm{f}}^2}\bar{\boldsymbol{C}}(i,:) \tag{77}$$

where $\bar{\boldsymbol{C}}(i,:)\ \ (1\le i\le n)$ denotes the *i*th row of the matrix. Taking the derivatives of Eq. (30) with respect to the sliding magnitude vector ($\boldsymbol{s}$) yields

$$\frac{\partial \boldsymbol{Q}_{\mathrm{e}}}{\partial \boldsymbol{s}}=\sum_{i=1}^{n}\left(\boldsymbol{C}_i\otimes\boldsymbol{I}_6\right)^{\mathrm{T}}\frac{EAh_i}{h_{i,\mathrm{f}}^2}\begin{bmatrix}-\boldsymbol{B}_i^{\mathrm{T}}\hat{\boldsymbol{h}}_i\\ \boldsymbol{B}_{i+1}^{\mathrm{T}}\hat{\boldsymbol{h}}_i\end{bmatrix}\bar{\boldsymbol{C}}(i,:) \tag{78}$$

By using expressions (24), (35) and (56), we can derive the expression of the tangent matrix of the second part

$$\frac{\mathrm{d}\boldsymbol{Q}_{\mathrm{e}}}{\mathrm{d}\bar{\boldsymbol{s}}}=\frac{\partial \boldsymbol{Q}_{\mathrm{e}}}{\partial \boldsymbol{s}}\frac{\partial \boldsymbol{s}}{\partial \bar{\boldsymbol{s}}} \tag{79}$$

where $\partial\boldsymbol{s}/\partial\bar{\boldsymbol{s}}\in\Re^{(n-1)\times 2(n-1)}$ is given as

$$\frac{\partial \boldsymbol{s}}{\partial \bar{\boldsymbol{s}}}=\begin{bmatrix}1 & -1 & & & & \\ & 1 & -1 & & & \\ & & & \ldots & \ldots & \\ & & & & 1 & -1\end{bmatrix} \tag{80}$$

B.3 The third part $\mathrm{d}\boldsymbol{\Psi}/\mathrm{d}\boldsymbol{q}$

Note from Eqs. (53)~(55) that we have the following relationship

$$\frac{\mathrm{d}\boldsymbol{\Psi}}{\mathrm{d}\boldsymbol{q}}=\frac{\partial \boldsymbol{\Psi}}{\partial \boldsymbol{\varsigma}}\frac{\partial \boldsymbol{\varsigma}}{\partial \boldsymbol{q}} \tag{81}$$

where $\partial\boldsymbol{\Psi}/\partial\boldsymbol{\varsigma}\in\Re^{2(n-1)\times 2(n-1)}$ is a diagonal matrix.

$$\frac{\partial \boldsymbol{\Psi}}{\partial \boldsymbol{\varsigma}}=\mathrm{diag}\left[\frac{\partial \psi_2^+}{\partial \varsigma_2^+},\frac{\partial \psi_2^-}{\partial \varsigma_2^-},\cdots,\frac{\partial \psi_n^+}{\partial \varsigma_n^+},\frac{\partial \psi_n^-}{\partial \varsigma_n^-}\right] \tag{82}$$

By using Eq. (53), the item $\partial\psi_i^{\pm}/\partial\varsigma_i^{\pm}\ \ (2\le i\le n)$ above can be given as

$$\frac{\partial \psi_i^{\pm}}{\partial \varsigma_i^{\pm}}=\frac{\varsigma_i^{\pm}}{\chi_1^2\sqrt{\left(\varsigma_i^{\pm}/\chi_1\right)^2+\left(\chi_2 s_i^{\pm}\right)^2+2\varepsilon^2}}-\frac{1}{\chi_1} \tag{83}$$

To obtain the item $\partial\boldsymbol{\varsigma}/\partial\boldsymbol{q}$, we can first define a tension magnitude vector,

Journal Pre-proofs

$$\boldsymbol{F}=\begin{bmatrix}F_1 & F_2 & \cdots & F_n\end{bmatrix}^{\mathrm{T}} \tag{84}$$

and can establish the relationship between $\boldsymbol{\varsigma}$ and $\boldsymbol{F}$ by using Eqs. (37) and (55),

$$\boldsymbol{\varsigma}=\boldsymbol{\Lambda}\boldsymbol{F} \tag{85}$$

where matrix $\boldsymbol{\Lambda}\in\Re^{2(n-1)\times n}$ is given as

$$\boldsymbol{\Lambda}=\begin{bmatrix}
-1 & 1/\alpha_2 & & & & \\
1 & -\alpha_2 & & & & \\
 & -1 & 1/\alpha_3 & & & \\
 & 1 & -\alpha_3 & & & \\
 & & \ddots & \ddots & & \\
 & & \ddots & \ddots & & \\
 & & & -1 & 1/\alpha_n \\
 & & & 1 & -\alpha_n
\end{bmatrix} \tag{86}$$

Strictly speaking, note from the sliding criterion (32) that $\boldsymbol{\Lambda}$ is a function of the contact angle (θ), and therefore is a function of the system configuration ($\boldsymbol{q}$). However, to avoid overly cumbersome operations, we ignore the variation of the sliding limit ratio α_i with respect to the system configuration ($\boldsymbol{q}$). This is particularly suitable for a multi-loading step analysis, where in each loading step the variation of the contact angle is very small. As a result, we have the expression

$$\frac{\partial\boldsymbol{\varsigma}}{\partial\boldsymbol{q}}=\boldsymbol{\Lambda}\frac{\partial\boldsymbol{F}}{\partial\boldsymbol{q}} \tag{87}$$

The expression of $\partial\boldsymbol{F}/\partial\boldsymbol{q}$ is given as

$$\frac{\partial\boldsymbol{F}}{\partial\boldsymbol{q}}=\begin{bmatrix}\left(\dfrac{\partial F_1}{\partial\boldsymbol{q}}\right)^{\mathrm{T}} & \left(\dfrac{\partial F_2}{\partial\boldsymbol{q}}\right)^{\mathrm{T}} & \cdots & \left(\dfrac{\partial F_n}{\partial\boldsymbol{q}}\right)^{\mathrm{T}}\end{bmatrix}^{\mathrm{T}} \tag{88}$$

where $\partial F_i/\partial\boldsymbol{q}\ (1\le i\le n)$ can be obtained by using Eq. (71), as

$$\frac{\partial F_i}{\partial\boldsymbol{q}}=\begin{bmatrix}\dfrac{\partial F_i}{\partial\boldsymbol{q}_p} & \dfrac{\partial F_i}{\partial\boldsymbol{q}_q}\end{bmatrix}\left(\boldsymbol{C}_i\otimes\boldsymbol{I}_6\right)=\frac{EA\hat{\boldsymbol{h}}_i^{\mathrm{T}}}{h_{i,\mathrm{f}}}\begin{bmatrix}\boldsymbol{B}_i & -\boldsymbol{B}_{i+1}\end{bmatrix}\left(\boldsymbol{C}_i\otimes\boldsymbol{I}_6\right) \tag{89}$$

B.4 The fourth part $\mathrm{d}\boldsymbol{\Psi}/\mathrm{d}\overline{\boldsymbol{s}}$

Taking the derivation of Eq. (54) with respect to the sliding assistant vector ($\overline{\boldsymbol{s}}$) yields

Journal Pre-proofs

$$\frac{\mathrm{d}\boldsymbol{\Psi}}{\mathrm{d}\overline{\boldsymbol{s}}}=\frac{\partial\boldsymbol{\Psi}}{\partial\boldsymbol{\varsigma}}\frac{\partial\boldsymbol{\varsigma}}{\partial\overline{\boldsymbol{s}}}+\frac{\partial\boldsymbol{\Psi}}{\partial\overline{\boldsymbol{s}}} \tag{90}$$

where $\partial\boldsymbol{\Psi}/\partial\boldsymbol{\varsigma}$ is given by Eq. (82) and $\partial\boldsymbol{\Psi}/\partial\overline{\boldsymbol{s}}$ is a diagonal matrix given as

$$\frac{\partial\boldsymbol{\Psi}}{\partial\overline{\boldsymbol{s}}}=\mathrm{diag}\left[\frac{\partial\psi_2^+}{\partial s_2^+},\frac{\partial\psi_2^-}{\partial s_2^-},\cdots,\frac{\partial\psi_n^+}{\partial s_n^+},\frac{\partial\psi_n^-}{\partial s_n^-}\right] \tag{91}$$

By using Eq. (53), the expressions of $\partial\psi_i^{\pm}/\partial\varsigma_i^{\pm}$ $\left(1\le i\le n\right)$ above can be given as

$$\frac{\partial\psi_i^{\pm}}{\partial s_i^{\pm}}=\frac{\chi_2^2 s_i^{\pm}}{\sqrt{\left(\varsigma_i^{\pm}/\chi_1\right)^2+\left(\chi_2 s_i^{\pm}\right)^2+2\varepsilon^2}}-\chi_2 \tag{92}$$

The remaining task is to obtain the expression of $\partial\boldsymbol{\varsigma}/\partial\overline{\boldsymbol{s}}$ in Eq. (90), which can be given by using Eq. (85) as

$$\frac{\partial\boldsymbol{\varsigma}}{\partial\overline{\boldsymbol{s}}}=\boldsymbol{\Lambda}\frac{\partial\boldsymbol{F}}{\partial\overline{\boldsymbol{s}}}=\boldsymbol{\Lambda}\frac{\partial\boldsymbol{F}}{\partial\boldsymbol{s}}\frac{\partial\boldsymbol{s}}{\partial\overline{\boldsymbol{s}}} \tag{93}$$

The expression of $\partial\boldsymbol{s}/\partial\overline{\boldsymbol{s}}$ is given by Eq. (80), and $\partial\boldsymbol{F}/\partial\boldsymbol{s}$ can be obtained by

$$\frac{\partial\boldsymbol{F}}{\partial\boldsymbol{s}}=\left[\left(\frac{\partial F_1}{\partial\boldsymbol{s}}\right)^{\mathrm{T}}\ \left(\frac{\partial F_2}{\partial\boldsymbol{s}}\right)^{\mathrm{T}}\ \cdots\ \left(\frac{\partial F_n}{\partial\boldsymbol{s}}\right)^{\mathrm{T}}\right]^{\mathrm{T}} \tag{94}$$

where $\partial F_i/\partial\boldsymbol{s}$ $\left(1\le i\le n\right)$ has been given by Eq. (77).

C. Some key terms in computing the generalized force vector and the tangent matrices

As mentioned previously, to obtain the exact tangent matrices of the clustered cables, one should evaluate the term $\partial\left(\boldsymbol{B}^{\mathrm{T}}\boldsymbol{V}_3\right)/\partial\boldsymbol{q}$ (see Eq. (73); subscripts for the body index are omitted for brevity). For convenience of numerical calculations, in this paragraph detailed expressions of the matrix are given in a component manner.

The global position of the origin of the local coordinate system fixed on the rigid body is $\boldsymbol{R}=\left[x,y,z\right]^{\mathrm{T}}$, and the orientation of the local coordinate frame is described by the classical Euler angle, which denotes $\boldsymbol{\Theta}=\left[\psi,\theta,\varphi\right]^{\mathrm{T}}$; the generalized coordinates of the rigid body are $\boldsymbol{q}=\left[\boldsymbol{R}^{\mathrm{T}},\boldsymbol{\Theta}^{\mathrm{T}}\right]^{\mathrm{T}}$. The vector of the connection point of a classical or clustered cable to the body is defined as $\boldsymbol{u}'=\left[u_x,u_y,u_z\right]^{\mathrm{T}}$. Define $\boldsymbol{V}_n=\left[v_1,v_2,\cdots,v_n\right]^{\mathrm{T}}$ as an arbitrary *n*-dimensional column vector.

C.1 Expressions of matrix $\boldsymbol{B}\in\Re^{3\times6}$

Journal Pre-proofs

$$
\begin{aligned}
&\boldsymbol{B}(1,1)=1;\ \boldsymbol{B}(2,2)=1;\ \boldsymbol{B}(3,3)=1;\\
&\boldsymbol{B}(1,4)=u_y\left(\mathrm{s}_\varphi \mathrm{s}_\psi-\mathrm{c}_\varphi \mathrm{c}_\psi \mathrm{c}_\theta\right)-u_x\left(\mathrm{c}_\varphi \mathrm{s}_\psi+\mathrm{c}_\psi \mathrm{c}_\theta \mathrm{s}_\varphi\right)+u_z \mathrm{c}_\psi \mathrm{s}_\theta;\\
&\boldsymbol{B}(1,5)=u_z \mathrm{c}_\theta \mathrm{s}_\psi+u_y \mathrm{c}_\psi \mathrm{s}_\psi \mathrm{s}_\theta+u_x \mathrm{s}_\varphi \mathrm{s}_\psi \mathrm{s}_\theta;\\
&\boldsymbol{B}(1,6)=-u_x\left(\mathrm{c}_\psi \mathrm{s}_\varphi+\mathrm{c}_\varphi \mathrm{c}_\theta \mathrm{s}_\psi\right)-u_y\left(\mathrm{c}_\varphi \mathrm{c}_\psi-\mathrm{c}_\theta \mathrm{s}_\varphi \mathrm{s}_\psi\right);\\
&\boldsymbol{B}(2,4)=u_x\left(\mathrm{c}_\varphi \mathrm{c}_\psi-\mathrm{c}_\theta \mathrm{s}_\varphi \mathrm{s}_\psi\right)-u_y\left(\mathrm{c}_\psi \mathrm{s}_\varphi+\mathrm{c}_\varphi \mathrm{c}_\theta \mathrm{s}_\psi\right)+u_z \mathrm{s}_\psi \mathrm{s}_\theta;\\
&\boldsymbol{B}(2,5)=-u_z \mathrm{c}_\psi \mathrm{c}_\theta-u_y \mathrm{c}_\varphi \mathrm{c}_\psi \mathrm{s}_\theta-u_x \mathrm{c}_\psi \mathrm{s}_\varphi \mathrm{s}_\theta;\\
&\boldsymbol{B}(2,6)=-u_x\left(\mathrm{s}_\varphi \mathrm{s}_\psi-\mathrm{c}_\varphi \mathrm{c}_\psi \mathrm{c}_\theta\right)-u_y\left(\mathrm{c}_\varphi \mathrm{s}_\psi+\mathrm{c}_\psi \mathrm{c}_\theta \mathrm{s}_\varphi\right);\\
&\boldsymbol{B}(3,5)=u_y \mathrm{c}_\varphi \mathrm{c}_\theta-u_z \mathrm{s}_\theta+u_x \mathrm{c}_\theta \mathrm{s}_\varphi;\\
&\boldsymbol{B}(3,6)=u_x \mathrm{c}_\varphi \mathrm{s}_\theta-u_y \mathrm{s}_\varphi \mathrm{s}_\theta;
\end{aligned}
\tag{95}
$$

C.2 Expressions of matrix $\boldsymbol{T}=\partial\left(\boldsymbol{B}^{\mathrm{T}}\boldsymbol{V}_3\right)/\partial\boldsymbol{q}\in\Re^{6\times 6}$

$$
\begin{aligned}
\boldsymbol{T}(4,4)&=v_2\left(u_y\left(\mathrm{s}_\varphi \mathrm{s}_\psi-\mathrm{c}_\varphi \mathrm{c}_\psi \mathrm{c}_\theta\right)-u_x\left(\mathrm{c}_\varphi \mathrm{s}_\psi+\mathrm{c}_\psi \mathrm{c}_\theta \mathrm{s}_\varphi\right)+u_z \mathrm{c}_\psi \mathrm{s}_\theta \mathrm{s}_\theta\right)\cdots\\
&\quad -v_1\left(u_x\left(\mathrm{c}_\varphi \mathrm{c}_\psi-\mathrm{c}_\theta \mathrm{s}_\varphi \mathrm{s}_\psi\right)-u_y\left(\mathrm{c}_\psi \mathrm{s}_\varphi+\mathrm{c}_\varphi \mathrm{c}_\theta \mathrm{s}_\psi\right)+u_z \mathrm{s}_\psi \mathrm{s}_\theta\right);\\
\boldsymbol{T}(4,5)&=v_1\left(u_z \mathrm{c}_\psi \mathrm{c}_\theta+u_y \mathrm{c}_\varphi \mathrm{c}_\psi \mathrm{s}_\theta+u_x \mathrm{c}_\psi \mathrm{s}_\varphi \mathrm{s}_\theta\right)\cdots\\
&\quad +v_2\left(u_z \mathrm{c}_\theta \mathrm{s}_\psi+u_y \mathrm{c}_\varphi \mathrm{s}_\psi \mathrm{s}_\theta+u_x \mathrm{s}_\varphi \mathrm{s}_\psi \mathrm{s}_\theta\right);\\
\boldsymbol{T}(4,6)&=v_1\left(u_x\left(\mathrm{s}_\varphi \mathrm{s}_\psi-\mathrm{c}_\varphi \mathrm{c}_\psi \mathrm{c}_\theta\right)+u_y\left(\mathrm{c}_\varphi \mathrm{s}_\psi+\mathrm{c}_\psi \mathrm{c}_\theta \mathrm{s}_\varphi\right)\right)\cdots\\
&\quad -v_2\left(u_x\left(\mathrm{c}_\psi \mathrm{s}_\varphi+\mathrm{c}_\varphi \mathrm{c}_\theta \mathrm{s}_\psi\right)+u_y\left(\mathrm{c}_\varphi \mathrm{c}_\psi-\mathrm{c}_\theta \mathrm{s}_\varphi \mathrm{s}_\psi\right)\right);\\
\boldsymbol{T}(5,5)&=v_1\left(u_y \mathrm{c}_\varphi \mathrm{c}_\theta \mathrm{s}_\psi-u_z \mathrm{s}_\psi \mathrm{s}_\theta+u_x \mathrm{c}_\theta \mathrm{s}_\varphi \mathrm{s}_\psi\right)\cdots\\
&\quad -v_2\left(u_y \mathrm{c}_\varphi \mathrm{c}_\psi \mathrm{c}_\theta-u_z \mathrm{c}_\psi \mathrm{s}_\theta+u_x \mathrm{c}_\psi \mathrm{c}_\theta \mathrm{s}_\varphi\right)-v_3\left(u_z \mathrm{c}_\theta+u_y \mathrm{c}_\varphi \mathrm{s}_\theta+u_x \mathrm{s}_\varphi \mathrm{s}_\theta\right);\\
\boldsymbol{T}(5,6)&=v_1\left(u_x \mathrm{c}_\varphi \mathrm{s}_\psi \mathrm{s}_\theta-u_y \mathrm{s}_\varphi \mathrm{s}_\psi \mathrm{s}_\theta\right)\cdots\\
&\quad -v_2\left(u_x \mathrm{c}_\varphi \mathrm{c}_\psi \mathrm{s}_\theta-u_y \mathrm{c}_\psi \mathrm{s}_\varphi \mathrm{s}_\theta\right)+v_3\left(u_x \mathrm{c}_\varphi \mathrm{c}_\theta-u_y \mathrm{c}_\theta \mathrm{s}_\varphi\right);\\
\boldsymbol{T}(6,6)&=-v_1\left(u_x\left(\mathrm{c}_\varphi \mathrm{c}_\psi-\mathrm{c}_\theta \mathrm{s}_\varphi \mathrm{s}_\psi\right)-u_y\left(\mathrm{c}_\psi \mathrm{s}_\varphi+\mathrm{c}_\varphi \mathrm{c}_\theta \mathrm{s}_\psi\right)\right)\\
&\quad -v_2\left(u_x\left(\mathrm{c}_\varphi \mathrm{s}_\psi+\mathrm{c}_\psi \mathrm{c}_\theta \mathrm{s}_\varphi\right)-u_y\left(\mathrm{s}_\varphi \mathrm{s}_\psi-\mathrm{c}_\varphi \mathrm{c}_\psi \mathrm{c}_\theta\right)\right)-v_3\left(u_y \mathrm{c}_\varphi \mathrm{s}_\theta+u_x \mathrm{s}_\varphi \mathrm{s}_\theta\right);\\
\boldsymbol{T}(5,4)&=\boldsymbol{T}(4,5);\ \boldsymbol{T}(6,4)=\boldsymbol{T}(4,6);\ \boldsymbol{T}(6,5)=\boldsymbol{T}(5,6);
\end{aligned}
\tag{96}
$$

In the above expressions of matrices $\boldsymbol{B}$ and $\boldsymbol{T}$, we use the notations $\mathrm{c}_\chi=\cos(\chi)$ and $\mathrm{s}_\chi=\sin(\chi)$ $(\chi=\psi,\theta,\varphi)$, and all the components not given are equal to zero.

References

Adam, B., Smith, I.F.C., 2008. Active tensegrity: A control framework for an adaptive civil-engineering structure. Computers & Structures 86, 2215-2223.

Aloui, O., Floresa, J., Ordenb, D., Rhode-Barbarigos, L., 2019. Cellular morphogenesis of three-

Journal Pre-proofs

dimensional tensegrity structures. Comput Method Appl M 346, 85–108.
Baumgarte, J., 1972. Stabilization of constraints and integrals of motion in dynamical systems. Comput Method Appl M 1, 1-16.
Beer, F.B., Johnston, E.R., 1996. Vector mechanics for engineers: statics and dynamics. McGraw-Hill, New York.
Bel Hadj Ali, N., Kan, Z., Peng, H., Rhode-Barbarigos, L., 2019. On static analysis of tensile structures with sliding cables: the frictional sliding case. Eng Comput-germany.
Bel Hadj Ali, N., Rhode-Barbarigos, L., Smith, I.F.C., 2011. Analysis of clustered tensegrity structures using a modified dynamic relaxation algorithm. Int J Solids Struct 48, 637-647.
Bel Hadj Ali, N., Smith, I.F.C., 2010. Dynamic behavior and vibration control of a tensegrity structure. Int J Solids Struct 47, 1285-1296.
Bel Hadj Ali, N., Sychterz, A.C., Smith, I.F.C., 2017. A dynamic-relaxation formulation for analysis of cable structures with sliding-induced friction. Int J Solids Struct 126-127, 240-251.
Boulaud, R., Douthe, C., Sab, K., 2020. Modelling of curtain effect in rockfall barrier with the dynamic relaxation. Int J Solids Struct.
Brian R. Tietz, Ross W. Carnahan, Richard J. Bachmann, Roger D. Quinn, SunSpiral, V., 2013. Tetraspine: Robust Terrain Handling on a Tensegrity Robot Using Central Pattern Generators, 2013 IEEE/ASME International Conference on Advanced Intelligent Mechatronics (AIM), Wollongong, Australia.
Calladine, C.R., Pellegrino, S., 1991. First-order infinitesimal mechanisms. Int J Solids Struct 27, 505-515.
Cefalo, M., Mirats-Tur, J.M., 2011. A comprehensive dynamic model for class-1 tensegrity systems based on quaternions. Int J Solids Struct 48, 785-802.
Chen, Z.H., Wu, Y.J., Yin, Y., Shan, C., 2010. Formulation and application of multi-node sliding cable element for the analysis of Suspen-Dome structures. Finite Elem Anal Des 46, 743-750.
Cheong, J., Skelton, R.E., Cho, Y., 2014. A numerical algorithm for tensegrity dynamics with non-minimal coordinates. Mech Res Commun 58, 46-52.
Choo, Y.S., Ju, F., Lee, K.H., 1997. Static sling tensions in heavy lifts with doubled sling arrangement. International Journal of Offshore and Polar Engineering 7, 313-322.
Cottle, R.W., Pang, J.-S., Stone, R.E., 1992. The linear complementarity problem. Boston : Academic Press.
Coulibaly, J.B., Chanut, M.A., Lambert, S., Nicot, F., 2018. Sliding cable modeling: an attempt at a unified formulation. Int J Solids Struct 130-131, 1-10.
Fest, E., Shea, K., Smith, I.F.C., 2004. Active Tensegrity Structure. Journal of Structural Engineering 130, 1454-1465.
Fischer, A., 1992. A special newton-type optimization method. Optimization 24, 269-284.
Gan, B.S., Zhang, J., Nguyen, D.-K., Nouchi, E., 2015. Node-based genetic form-finding of irregular tensegrity structures. Comput Struct 159, 61-73.
Gao, W., Lu, X., 2019. Modelling unbonded prestressing tendons in self-centering connections through improved sliding cable elements. Eng Struct 180, 809-828.
Graells Rovira, A., Mirats Tur, J.M., 2009. Control and simulation of a tensegrity-based mobile robot. Robot Auton Syst 57, 526-535.
Hairer, E., Wanner, G., 2002. Solving ordinary differential equations II stiff and differential-algebraic problems. Springer-Verlag.
Ham, S.-H., Roh, M.-I., Lee, H., Hong, J.-W., Lee, H.-R., 2017. Development and validation of a simulation-based safety evaluation program for a mega floating crane. Adv Eng Softw 112, 101-116.

Ingber, D.E., 2003a. Tensegrity I. Cell structure and hierarchical systems biology. J Cell Sci 116, 1157-1173.

Ingber, D.E., 2003b. Tensegrity II. How structural networks influence cellular information processing networks. J Cell Sci 116, 1397-1408.

Jean, M., 1999. The non-smooth contact dynamics method. Comput Method Appl M 177, 235-257.

Ju, F., Choo, Y.S., 2005. Super element approach to cable passing through multiple pulleys. Int J Solids Struct 42, 3533-3547.

Juan, S.H., Mirats Tur, J.M., 2008. Tensegrity frameworks: static analysis review. Mech Mach Theory 43, 859-881.

Kan, Z., Li, F., Peng, H., Chen, B., Song, X., 2021. Sliding cable modeling: A nonlinear complementarity function based framework. Mech Syst Signal Pr 146, 107021.

Kan, Z., Peng, H., Chen, B., 2018a. Complementarity Framework for Nonlinear Analysis of Tensegrity Structures with Slack Cables. AIAA J. 56, 5013-5027.

Kan, Z., Peng, H., Chen, B., Zhong, W., 2018b. Nonlinear dynamic and deployment analysis of clustered tensegrity structures using a positional formulation FEM. Compos Struct 187, 241-258.

Kan, Z., Peng, H., Chen, B., Zhong, W., 2018c. A sliding cable element of multibody dynamics with application to nonlinear dynamic deployment analysis of clustered tensegrity. Int J Solids Struct 130-131, 61-79.

Kanchanasaratool, N., Williamson, D., 2002. Modelling and control of class NSP tensegrity structures. Int J Control 75, 123-139.

Kanzow, C., 1996. Some Noninterior Continuation Methods for Linear Complementarity Problems. Siam J Matrix Anal A 17, 851-868.

Kardas, D., Nackenhorst, U., Balzani, D., 2013. Computational model for the cell-mechanical response of the osteocyte cytoskeleton based on self-stabilizing tensegrity structures. Biomech Model Mechanobiol 12, 167-183.

Kebiche, K., Kazi-Aoual, M.N., Motro, R., 1999. Geometrical non-linear analysis of tensegrity systems. Eng Struct 21, 864-876.

Kwan, A.S.K., Pellegrino, S., 1994. Matrix formulation of macro-elements for deployable structures. Comput Struct 50, 237-254.

Lee, K.H., Choo, Y.S., Ju, F., 2003. Finite element modelling of frictional slip in heavy lift sling systems. Comput Struct 81, 2673-2690.

Lemke, C.E., 1965. Bimatrix Equilibrium Points and Mathematical Programming. Manage Sci 11, 681-689.

Liu, H., Han, Q., Chen, Z., Wang, X., Yan, R.-Z., Zhao, B., 2014. Precision control method for pre-stressing construction of suspen-dome structures. Advanced Steel Construction 10, 404-425.

Moored, K.W., Bart-Smith, H., 2009. Investigation of clustered actuation in tensegrity structures. Int J Solids Struct 46, 3272-3281.

Murakami, H., 2001. Static and dynamic analyses of tensegrity structures. Part 1. nonlinear equations of motion. Int J Solids Struct 38, 3599-3613.

Myers, T.W., 2009. Anatomy Trains: Myofascial Meridians for Manual and Movement Therapists (2nd Edition). Elsevier.

Nagase, K., Skelton, R.E., 2015. Double-Helix Tensegrity Structures. AIAA J. 53, 847-862.

Nishimura, Y., Murakami, H., 2001. Initial shape-finding and modal analyses of cyclic frustum tensegrity modules. Comput Method Appl M 190, 5795-5818.

Journal Pre-proofs

Pagitz, M., Mirats Tur, J.M., 2009. Finite element based form-finding algorithm for tensegrity structures. Int J Solids Struct 46, 3235-3240.

Pang, J.-S., Facchinei, F., 2003. Finite-Dimensional Variational Inequalities and Complementarity Problems. Springer, New York.

Paul, C., Cuevas, F.V., Lipson, H., 2006. Design and control of tensegrity robots for locomotion. IEEE Transactions on Robotics 22, 944-957.

Paul, C., Lipson, H., Cuevas, F.V., 2005. Gait production in a tensegrity based robot, International Conference on Advanced Robotics, pp. 216-222.

Peng, H., Li, F., Liu, J., Ju, Z., 2020. A Symplectic Instantaneous Optimal Control for Robot Trajectory Tracking With Differential-Algebraic Equation Models. Ieee T Ind Electron 67, 3819-3829.

Shabana, A.A., 2005. Dynamics of multibody systems, Third ed. Cambridge University Press.

Skelton, R.E., De Oliveira, M.C., 2009. Tensegrity systems. Springer.

Smaili, A., Motro, R., 2005. Folding/unfolding of tensegrity systems by removal of self-stress. In: IASS 2005 Symposium on Shell and Spatial Structures -Theory,Technique, Valuation, Maintenance. Bucarest, pp. 595–602.

Sultan, C., 2009. Tensegrity : 60 years of art, science, and engineering, Adv. Appl. Mech. Elsevier Science & Technology, pp. 60-145.

Sultan, C., Skelton, R., 2003. Deployment of tensegrity structures. Int J Solids Struct 40, 4637-4657.

Veuve, N., Safaei, S.D., Smith, I.F.C., 2015. Deployment of a tensegrity footbridge. Journal of Structural Engineering 141, 04015021.

Veuve, N., Safaei, S.D., Smith, I.F.C., 2016. Active control for mid-span connection of a deployable tensegrity footbridge. Eng Struct 112, 245-255.

Wroldsen, A.S., de Oliveira, M.C., Skelton, R.E., 2009. Modelling and control of non-minimal non-linear realisations of tensegrity systems. Int J Control 82, 389-407.

Wu, J., Zhang, L., He, Z., Yan, Z., 2019. Comparative Analysis of Two Tensegrity Grids Considering Slack and Rupture of Cables. AIAA J., 1-9.

Yang, S., Sultan, C., 2017. A comparative study on the dynamics of tensegrity-membrane systems based on multiple models. Int J Solids Struct 113-114, 47-69.

You, Z., Pellegrino, S., 1996. Cable-stiffened pantographic deployable structures part 1: triangular mast. AIAA J. 34, 813-820.

You, Z., Pellegrino, S., 1997. Cable-stiffened pantographic deployable structures part 2: mesh reflector. AIAA J. 35, 1348-1355.

Zhang, G., Dong, S., Zhuo, X., Guo, J., Zhao, X., 2008. Research on sliding cable in construction of suspend-dome structures. Journal of Zhejiang University (Engineering Science) 42, 1051-1057.

Zhang, L.-Y., Li, Y., Cao, Y.-P., Feng, X.-Q., 2014. Stiffness matrix based form-finding method of tensegrity structures. Eng Struct 58, 36-48.

Zhang, L., Gao, Q., Liu, Y., Zhang, H., 2016. An efficient finite element formulation for nonlinear analysis of clustered tensegrity. Eng Computation 33, 252-273.

Zhang, L., Lu, M.K., Zhang, H.W., Yan, B., 2015. Geometrically nonlinear elasto-plastic analysis of clustered tensegrity based on the co-rotational approach. Int J Mech Sci 93, 154-165.

Zheng, H., Li, X., 2015. Mixed linear complementarity formulation of discontinuous deformation analysis. Int J Rock Mech Min 75, 23-32.

Zhou, B., Accorsi, M.L., Leonard, J.W., 2004. Finite element formulation for modeling sliding cable elements. Comput Struct 82, 271-280.

Journal Pre-proofs

Journal Pre-proofs

Journal Pre-proofs